

pubs.acs.org/Macromolecules Article

Determination of Glass Transition Temperatures in Bulk and Micellar Nanoconfined Polymers Using Fluorescent Molecular Rotors as Probes for Changes in Free Volume

Seyoung Kim, Minhwan Lee, Hyun Chang Kim, YongJoo Kim,* Won Bo Lee,* and You-Yeon Won*



Cite This: https://doi.org/10.1021/acs.macromol.3c00968



ACCESS

Metrics & More

Article Recommendations

Supporting Information

ABSTRACT: Fluorescent molecular rotors embedded in polymer matrices can probe the local changes in the dynamics of the polymer matrix (such as the glass transition of polymers near interfaces/surfaces) that are not accessible from macroscopic measurements. Yet, there is little consensus as to how the fluorescence data should be analyzed, what property the fluorescence intensity actually represents, and what are appropriate/optimal rotors for glass transition measurements. By experimentation with a model fluorescent rotor, farnesyl-(2-carboxy-2-cyanovinyl)-julolidine (FCVJ), and also re-analysis of data available in the literature for other types of molecular rotors, we investigated the correlation between the relaxation processes of

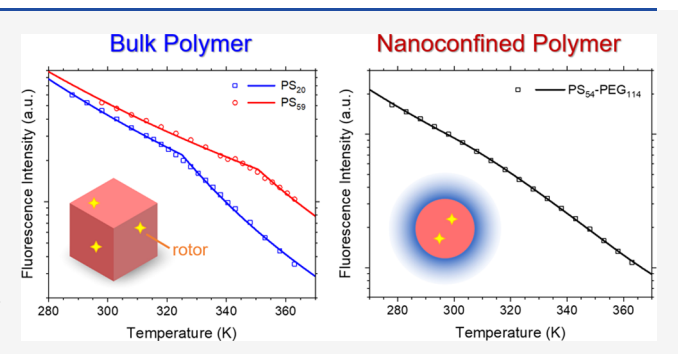


photo-excited rotors and free volume changes in matrix polymers. The temperature dependences of the fluorescence intensities from FCVJ-doped polystyrene (PS), poly(vinyl acetate) (PVAc), and poly(isobutyl methacrylate) (PiBMA) materials across their glass transition temperatures ($T_{\rm g}$) were successfully modeled using a free volume model which is based on the original theory of Loutfy that relates the fluorescence of a rotor probe to the free volume of the matrix, and the revised definition of the total free volume quantity proposed by Lipson and White (the Locally Correlated Lattice model-based free volume) that includes both the vibrational free volume and the excess free volume. Atomistic molecular dynamics simulation supports that the timescale of the vibrational motion of PS monomers is comparable to the intrinsic timescale of a rotor's internal rotation known in the literature (on the order of picoseconds), and thus the rotation of a rotor is controlled by the friction from the hard-core volume (not by the friction from the vibrational volume) of the monomers. Measurements on FCVJ-loaded polystyrene—poly(ethylene glycol) (PS—PEG) micelles in water suggest that the PS core domain of the PS—PEG micelle has a broad distribution of glass transition temperatures; a quantitative analysis based on the free volume model enabled to estimate the actual range of $T_{\rm g}$. These results allow us to conclude that fluorescent molecular rotors with a tendency toward rapid non-radiative (rotational) relaxation and bulky rotating subgroups (such as FCVJ) exhibit a strong coupling between the fluorescence of the rotor and the free volume of the matrix and are thus useful probes for $T_{\rm g}$ measurements.

INTRODUCTION

Fluorescent molecular rotors represent a specific category of fluorescent probes. The non-radiative relaxation of photoexcited molecular rotors involves mechanical internal rotation of the rotor molecules. Since the rotor's rotation is influenced by local friction, molecular rotors can be used as probes for measurements of free volume-related properties. Molecular rotors have been successfully applied to measurements of, for instance, viscosities of small molecular fluids, and physical aging in polymeric materials. Molecular rotors have also been shown to be useful for probing the microscale spatial variation in free volume in glassy polymers under mechanical deformation.

For the determination of the glass transition temperatures $(T_g$'s) of polymers, however, conventional fluorescent probes (non-rotor fluorophores such as pyrene) have been more

commonly used. Fluorescent probes have been particularly useful for the investigation of the local $T_{\rm g}$ properties of nanoconfined polymers. Pyrene is the most commonly used fluorescent probe for such measurements. However, pyrene has limited utility; it only works for certain polymers. Unlike molecular rotors which undergo an internal transition from the excited singlet (S_1) to the ground state (S_0) , the major route of non-radiative decay of pyrene probes is via intersystem crossing from the excited singlet (S_1) to the excited triplet

Received: May 17, 2023 **Revised:** July 14, 2023



 $(T_1)^{;13,14}$ this process involves quantum chemical interactions between the probe and the matrix and therefore depends on chemical specificity. To the contrary, molecular rotors are more generally applicable to a wide range of polymer types, because their non-radiative relaxation mechanism involves internal rotation of the probe molecules which is closer to a classical mechanical process. Further, relative to molecular rotors (as discussed below), the quantitative relationship between the fluorescence quantum yield and the matrix free volume is far less understood for pyrene and other non-rotor-type fluorescent probes. Therefore, there are advantages of using molecular rotors for polymer $T_{\rm g}$ measurements.

How a molecular rotor's fluorescence is related to the free volume of the matrix has long been discussed in the literature. About 40 years ago, Loutfy first proposed a simple model for the relationship between the fluorescence quantum yield (Φ) of a molecular rotor and the fractional free volume of the surrounding material (f); in the limit that the internal rotation is the rate-determining step for the non-radiative relaxation

$$\Phi \equiv k_{\rm r}/(k_{\rm r} + k_{\rm nr}) \cong k_{\rm r}/k_{\rm nr} \cong (k_{\rm r}/k_{\rm rot}^{\,0}) \exp(xf_0/f) \tag{1}$$

where k_r is the rate constant for radiative decay of the probe within the matrix, k_{nr} is the rate constant for non-radiative decay (and is typically much greater than k_r when the matrix is non-glassy or only slightly glassy), k_{rot}^{0} is the rate constant for internal rotation in vacuum, f_0 is the fraction of the occupied (van der Waals) volume (= 1 - f), and x is the so-called coupling parameter (which conceptually represents the fraction of rotor molecules that are coupled to matrix relaxation processes¹⁵ and is typically used as an adjustable parameter in fitting analysis).3,16 This model is analogous to the Doolittle model for viscosity $(\eta = \eta_0 \exp(yf_0/f))$, where y is an equivalent of the coupling parameter). Basically, the Loutfy model expresses that the rate of non-radiative decay (i.e., internal rotation) of a photo-exited rotor (k_{nr}) is retarded due to friction with the surrounding molecules ($\sim f_0/f$), that is, $k_{\rm nr}$ = $k_{\rm rot}^{0} \exp(-xf_0/f)$. Therefore, this model enables to relate the fluorescence from embedded rotor probes to free volumerelated properties of the matrix material (such as viscosity).³

Several reports are available in the literature demonstrating the use of molecular rotors for the determination of the $T_{\rm g}$'s of polymers. 6,15,16,18,19 Different procedures were applied to the data to determine the $T_{\rm g}$ for the polymer. In 1981, Loutfy reported that the log-linear plot of fluorescence intensity vs. temperature for poly(methyl methacrylate) (PMMA) loaded with benzylidenemalononitrile-based rotors shows a slope break at the $T_{\rm g}$ of the PMMA; specifically, the slope of the curve became more negative as the temperature was lowered below T_g . However, such a trend has not been observed in other studies. In analyzing fluorescence intensity of auramine O in poly(vinyl acetate) (PVAc) vs. temperature data, Meyer et al. defined the fictive T_g as the intersection of two extrapolating linear expansion lines from above and below the glass transition range. The same $T_{\rm g}$ determination procedure has also been used for other rotor/polymer combinations. ^{18,19} However, this bilinear analysis procedure has no theoretical basis, and it is, in fact, inconsistent with the Loutfy model (eq 1) which does not predict a linear limiting dependence of fluorescence on temperature; that is, $d\Phi/dT \neq constant$. Hooker and Torkelson showed that at $T > T_g$ the temperature dependence of a rotor's fluorescence intensity can be quantitively modeled with the Williams-Landel-Ferry

(WLF) theory (i.e., $\ln(\eta(T)/\eta(T_{\rm g}))$ (=(y/x)\ln($\Phi(T)/\Phi(T_{\rm g})$)) = $-C_1^{\rm g}(T-T_{\rm g})/(C_2^{\rm g}+T-T_{\rm g})$, where $C_1^{\rm g}$ and $C_2^{\rm g}$ are the WLF parameters (used as fitting parameters)), whereas at $T < T_{\rm g}$ the fluorescence profile deviates from the WLF prediction; therefore, a polymer's $T_{\rm g}$ can be determined by this type of fitting analysis, that is, as the temperature at which the fluorescence intensity starts to deviate from the prediction extrapolated from the WLF fit to the liquid-state data. However, for reasons discussed later, this procedure yields relatively inaccurate estimates of $T_{\rm g}$. Further, in the WLF model, the temperature-dependent fractional free volume at $T > T_{\rm g}$ is assumed to follow the relation, $f(T) = f_{\rm g} + (\alpha_{\rm L} - \alpha_{\rm G})$ ($T - T_{\rm g}$) where $f_{\rm g}$ is the fractional free volume at $T_{\rm g}$ and $\alpha_{\rm L}$ and $\alpha_{\rm G}$ are the thermal expansion coefficients of the liquid and glassy states of the polymer, respectively. Since the WLF theory uses this "excess-type" free volume definition ($V_{\rm f,exc}$, Figure 1)²⁰ (in other words, since $\alpha_{\rm G} \neq 0$), it inherently

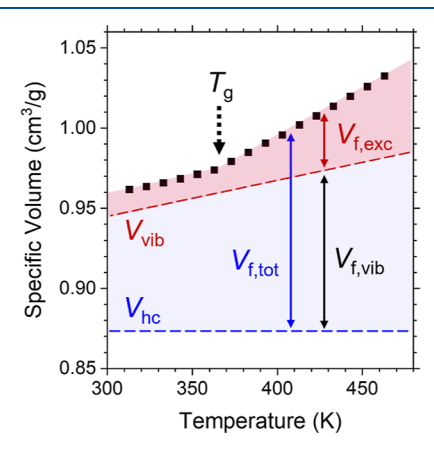


Figure 1. Illustration demonstrating the two different definitions of free volume ($V_{\rm f,tot}$ vs. $V_{\rm f,exc}$). White and Lipson defined the "total" free volume ($V_{\rm f,tot}$) as $V_{\rm f,exc} \equiv V - V_{\rm hc}$ where $V_{\rm hc}$ is the hard-core volume which can be estimated, for instance, using the LCL equation-of-state analysis of experimental PVT data. Conventionally, the free volume is defined as $V_{\rm f,exc} \equiv V - V_{\rm vib}$ where $V_{\rm vib}$ is the vibration volume (also called in the literature as the "occupied" volume); to distinguish from $V_{\rm f,tov}$ this type of free volume ($V_{\rm f,exc}$) has been described as the "excess" free volume. The WLF theory adopts this latter definition of free volume, and as a result, the free volume is thought to be a constant quantity in the glassy state (at $T < T_{\rm g}$). The difference between $V_{\rm hc}$ and $V_{\rm vib}$ is the "vibrational" free volume ($V_{\rm f,vib}$). Data (points and lines in the above diagram) represent those of polystyrene (PS) taken from ref 20.

suggests that at $T < T_g$, $f(T) = V_{f,exc}/V = f_g$ (const.), and therefore, within this theory, $\Phi(T)$ is also expected to be constant at $T < T_g$, which is in contradiction to experimental results (as shown in Figures 3 and 5, for instance, typically, Φ continues to increase with decreasing T even when $T < T_g$). To our knowledge, no attempts have previously been reported to model the temperature-dependent fluorescence $\Phi(T)$ of a molecular rotor over the entire range of T covering both above and below the matrix T_g .

In this article, we attempt to address this gap. Specifically, we show that the Loutfy model can quantitatively capture the temperature-dependent fluorescence behavior of molecular rotors over a wide temperature range, both above and below the $T_{\rm g}$, when used in combination with the Locally Correlated Lattice (LCL) model-based free volume definition proposed by White and Lipson.²⁰ White and Lipson calculated the

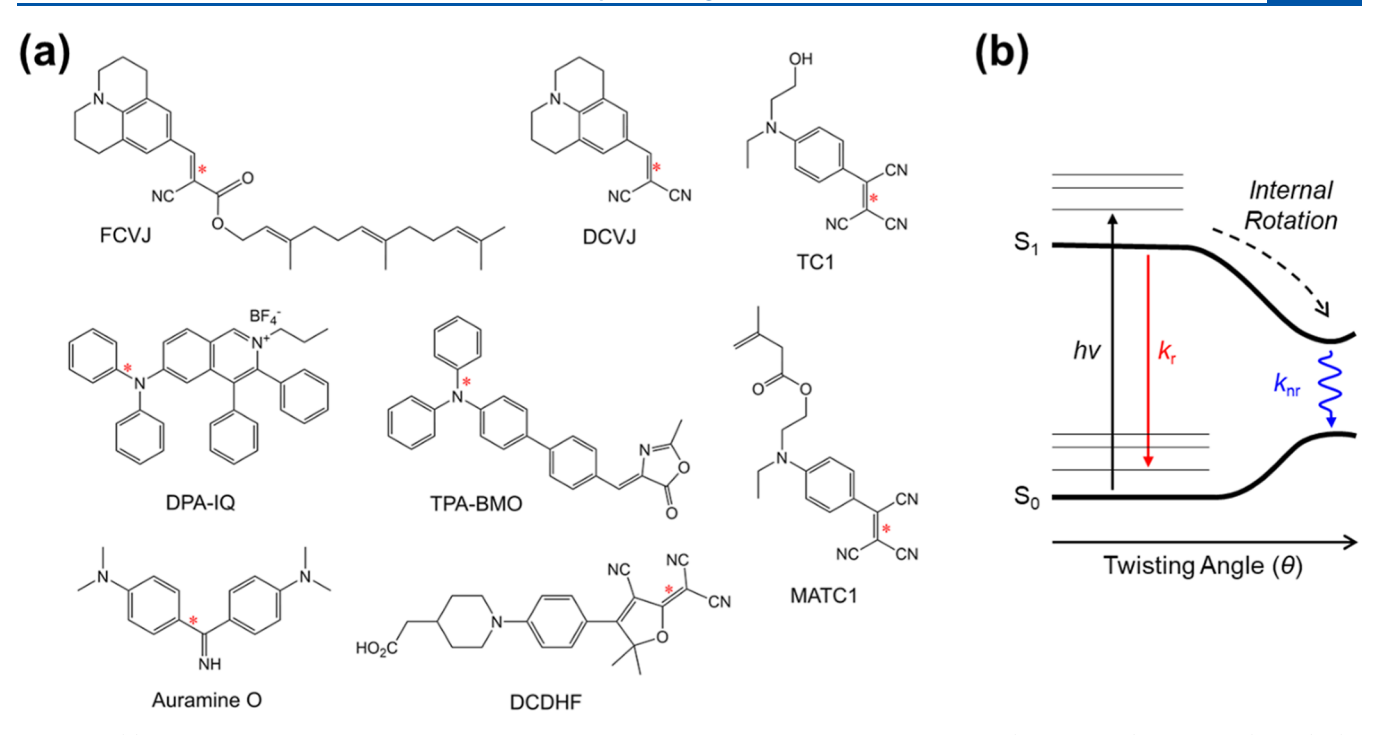


Figure 2. (a) Chemical structures of the fluorescent molecular rotors discussed in this article: FCVJ, 9-(dicyanovinyl)-julolidine (DCVJ), (4-(tricyanovinyl)-N-(2-hydroxyethyl)-N-ethyl)aniline (TC1), diphenylamine diphenylisoquinolinium (DPA-IQ), triphenylamine benzylidenemethyloxazolinone (TPA-BMO), (4-(tricyanovinyl)-N-(2-methacryloxyethyl)-N-ethyl)aniline (MATC1), bis(p-dimethylaminophenyl)methanimine (auramine O), and a dicyanodihydrofuran (DCDHF) derivative. The major axes of rotation (non-radiative relaxation) of photo-excited rotors are marked with asterisks. $^{23-27}$ (b) A schematic diagram explaining the mechanism of non-radiative relaxation of photo-excited molecular rotors from the excited singlet (S_1) to the ground state (S_0) (shown along the coordinate of the twisting angle of a rotor molecule); multiple vibrational states are present. After photonic excitation ($h\nu$), electron decay occurs by either the radiative (k_r) or non-radiative (k_{nr}) process. Typically, internal rotation is the rate-limiting step of the non-radiative relaxation for julolidine rotors; therefore, $k_{nr} \cong k_{rot}$.

incompressible hard-core volume (V_{hc}) using the LCL model (which is a thermodynamic equation-of-state model) and used the $V_{\rm hc}$ to calculate the total free volume $V_{\rm f,tot}$ ($\equiv V-V_{\rm hc}$) (Figure 1). Based on this free volume definition, they showed that, for a wide range of polymers, $f_{\rm g}$ (the fractional free volume at T_g) is a linearly varying function of T_g , which provides an explanation as to why f_g is not a universal parameter of all polymers but instead it varies from polymer to polymer and thus supports the reasonableness of the LCLbased free volume definition. In the present study, we further found that the total free volume $(V_{f,tot})$ (instead of the excess free volume $(V_{\rm f,exc})$) of the matrix polymer is indeed the relevant free volume quantity that controls the fluorescence intensity (Φ) of the rotor probe. Within this interpretation, because f(T) (= V_{ftot}/V) varies with T even in the glassy state (at $T < T_{\sigma}$) (Figure 1), the Loutfy model now becomes capable of quantitatively describing the experimentally observed, temperature-dependent fluorescence behavior of molecular rotors for glassy matrices; note, under the conventional definition ($V_{\rm f,exc} \equiv V - V_{\rm vib}$), the fractional free volume is independent of T in the glassy state, that is, f(T) (= $V_{\rm f,exc}/V$) = $f_{\rm g}$ (const.) at $T < T_{\rm g}$ (Figure 1). Also of note, an alternative free volume model of Zaccone and Terentjev (f(T) = 1 - $\phi_{\rm g} {\rm exp}(\alpha(T_{\rm g}-T))$ where $\phi_{\rm g}$ is the "critical monomer packing fraction" at T_g , and α is the thermal expansion coefficient (= α_L (at $T > T_g$) or α_G (at $T < T_g$)) can capture the temperature-dependent variation of the f in the glassy state. However, this model assumes that $\phi_{\rm g}$ (= 1 $-f_{\rm g}$) is a universal constant (\cong 0.64), which is inconsistent with experimental results; the values of f_g (= $(\alpha_L - \alpha_G)C_2^g$ in the WLF theory) vary from

polymer to polymer. As discussed above, the LCL model-based free volume definition ($V_{\rm f,tot} \equiv V - V_{\rm hc}$) resolves this issue; the LCL model predicts that $f_{\rm g}$ correlates with the $T_{\rm g}$ of a polymer and is thus a chemistry-specific property.²⁰

In examining whether the Loutfy model (used in combination with the LCL model-based free volume definition) can precisely capture the temperature-dependent fluorescence behavior of molecular rotors, we used data representing various different rotor/polymer combinations; we used both our own data and also data from the literature. The chemical structures of all molecular rotors investigated in this study are presented in Figure 2a. Our own experimental data were generated using a specific molecular rotor, called farnesyl-(2-carboxy-2-cyanovinyl)-julolidine (FCVJ), which has a great photostability. 21 FCVJ has previously been demonstrated for the determination of the entanglement molecular weight of poly(propylene oxide).²² Polymers used in our experiments include PS (in the bulk state), poly(isobutyl methacrylate) (PiBMA, in the bulk state), PVAc (in the bulk state) and poly(styrene)-poly(ethylene glycol) (PS-PEG, in the form of aqueous micelles having a 20 nm core diameter). We found that in all cases the rotor's fluorescence can be quantitatively modeled (fitted) with the combination of the Loutfy model and LCL model-based total free volume estimates over a temperature range, both above and below the $T_{\rm g}$. In an effort to rationalize this result (i.e., to understand why the vibrational free volume (V_{vib}) has to be included in the free volume calculation ($V_{\rm f,tot} \equiv V - V_{\rm hc}$, Figure 1)), we performed atomistic molecular dynamics (MD) simulations. We found that the vibrational timescale of PS monomers is comparable to

Table 1. Molecular Characteristics of the Polymers Used in This Study

polymer ID	$M_{\rm n,NMR}^{a}~({ m kDa})$	DP_n	$M_{\rm n,GPC}^{}$ (kDa)	$M_{ m w}/{M_{ m n}}^{b}$	$\alpha_{\rm G}^{\ c} \ (10^{-4} \ {\rm K}^{-1})$	$\alpha_{\rm L}^{\ c} \ (10^{-4} \ {\rm K}^{-1})$	$C_2^g(K)$	$f_{ m g,WLF}^{d}$
PS ₂₀	2.47	19.8 ^a	2.78	1.07	2.6^{20}	6.2 ²⁰	57.1 ³¹	0.016
PS ₅₉	6.60	59.4 ^a	7.35	1.10	2.6^{20}	6.2^{20}	57.1 ³¹	0.016
$PiBMA_{24}$	3.40	23.9 ^a	1.83	1.17	3.8^{32}	6.1 ³²		0.030 ^e
PVAc ₅₀₆		505.7 ^b	43.54	1.96	2.1 ³³	6.0^{33}	65.7^{34}	0.026
PS_{54} - PEG_{114}	11.01	54.0 ^a (PS)	11.66	1.16	2.6^{20}	6.2^{20}	57.1 ³¹	0.016

^aThe number-average molecular weight (including the end group molecular weights) $(M_{n,NMR})$ and the number-average degree of polymerization $(DP_{n,NMR})$ of a polymer were determined by ${}^{1}H$ NMR spectroscopy (i.e., from the area ratio between the main chain and end group signals); in the polymer ID, the subscript number represents the $DP_{n,NMR}$ value. See Figures S5a and S6a of the Supporting Information for the end group structures of the RAFT-synthesized PS and PiBMA polymers. ${}^{b}The$ number-average molecular weight $(M_{n,GPC})$, the number-average degree of polymerization $(DP_{n,GPC})$, and the overall molecular weight polydispersity index (M_w/M_n) were determined by gel permeation chromatography (GPC) (based on PS standards). ${}^{c}The$ values of the thermal expansion coefficients of the glassy and liquid states of the polymers $(\alpha_G$ and α_L , respectively) taken from the literature; for PiBMA, the α values were not available in the literature, and the reported values of α_G and α_L for poly(n-butyl methacrylate) were used. ${}^{d}The$ fractional free volume at T_g estimated using the equation $f_{g,WLF} = (\alpha_L - \alpha_G)C_2^g$ where C_2^g is the second WLF parameter. ${}^{e}f_{g,WLF}$ was calculated using the equation $f_{g,WLF} = (\alpha_L - \alpha_G)C_2^g$ where C_2^g is the second WLF parameter estimated for a reference temperature of T_r (≠ T_g); for PiBMA, $C_2 = 160$ K for $T_r = 358$ K, and $T_g = 331$ K.

Table 2. Glass Transition Temperatures $(T_{\rm g})$ of Different Polymers Determined by FCVJ Fluorescence and DSC Measurements

		Loutfy-LCL fit ^b			Lo			
polymer ID	Ex/Em^a (nm)	T _{g,LCL} (K)	x	C'	T _{g,WLF} (K)	x	C'	$T_{g,DSC}^{d}(K)$
PS_{20}	490/524	325	0.82	-5.73	331	0.06	-0.82	326
PS ₅₉	475/508	350	0.76	-4.61	350	0.03	0.78	353
$PiBMA_{24}$	459/496	310	0.37	-2.03	310	0.12	-1.86	305
PVAc ₅₀₆	481/499	314	0.47	-0.71	322	0.07	1.65	307
PS_{54} - PEG_{114}	475/508	$298 - 357^e$	0.73	-8.48				

"Excitation/emission wavelengths used for FCVJ fluorescence illumination/detection; the $T_{\rm g}$ was determined using data obtained during cooling at a rate of 0.5 K/min. "FCVJ fluorescence data were fit to the Loutfy model on the basis of the LCL model-based total free volume definition ($V_{\rm f,tot}$) using $T_{\rm g}$ (" $T_{\rm g,LCL}$ "), x (coupling parameter) and C' (intensity scale factor) as fitting variables. "FCVJ fluorescence data were fit to the Loutfy model on the basis of the WLF model-type excess free volume definition ($V_{\rm f,exc}$) using $T_{\rm g,WLF}$, x and C' as fitting variables. "The $T_{\rm g}$ was determined by DSC using data obtained during cooling at a rate of 5 K/min. "The range of $T_{\rm g}$ determined for the PS core domains of PS-PEG micelles dispersed in water (Figure 6).

the known rotational timescale of FCVJ (picoseconds); therefore, the vibrational monomer volume (V_{vib}) should be included in the free volume available for the FCVJ molecules to do rotational motion in. In the PS-PEG micelle situation, we found that the FCVJ fluorescence cannot be modeled with the Loutfy-LCL model if we assume that the PS core has a single glass transition, which suggests that due to its small size, the micelle core has a distribution of $T_{\rm g}$ values. Overall, our results support that the T_g of a polymer, whether in the bulk or nano-confined form, can be precisely determined by analysis of a rotor probe's fluorescent behavior using the combination of the Loutfy model and the LCL model-based free volume definition. On the other hand, we found that the conventional bilinear slope analysis procedure is able to give a reasonably accurate estimate of T_g only when the slope analysis is done on a log-linear (instead of linear-linear) plot of fluorescence intensity vs. temperature.

RESULTS AND DISCUSSION

Fluorescence from FCVJ-Doped Polymers. The PS_{20} , PS_{59} , and $PiBMA_{24}$ homopolymers used in this study were synthesized by reversible addition—fragmentation (chain) transfer polymerization (RAFT); in the polymer notations, the subscript numbers denote the number-average degree of polymerization (DP_n) values of the polymers. These polymers were measured to have relatively narrow molecular weight distributions ($M_w/M_n < 1.2$ as determined by GPC). The $PVAc_{506}$ sample ($M_{n,GPC} = 43.5 \text{ kDa}$) was purchased from a

commercial vendor (Alfa Aesar). The molecular characteristics of these polymers are summarized in Table 1. FCVJ (synthesized in-house) was dispersed in polymers at a low concentration (0.01 wt %) to avoid aggregation. Upon photoexcitation, FCVJ relaxes by emitting light and/or by undergoing a non-radiative transition via internal rotation/conversion similarly to other julolidine-based rotors (Figure 2b). The axis of internal rotation is the double bond between the planar julolidine headgroup and the long farnesyl ester tail (Figure 2a); photo-excitation turns the π bonding molecular orbital (π) of the double bond into a π antibonding molecular orbital (π *), and the stabilization in going from the π * back to π orbital generates internal rotation of the FCVJ molecule. ^{24,29}

The fluorescence spectra of FCVJ embedded in the polymer matrices were measured at respective maximum excitation wavelengths (Table 2). The fluorescence intensity (I) increased with decreasing temperature (T), while the maximum emission wavelength remained nearly unchanged with temperature (Figure S1). Typically, cooling of the polymer below its $T_{\rm g}$ in a glass cuvette caused the formation of microcracks within the polymer sample (because of a mismatch in thermal expansivity between the polymer and the cuvette), resulting in a discontinuous drop in fluorescence reading (due to a decrease in transmittance) as shown in Figure 3 (filled circles) and Figure S1. Because the cracks should not affect the local dynamics of the polymer chains, the low temperature portion of the I-T curve (i.e., the portion

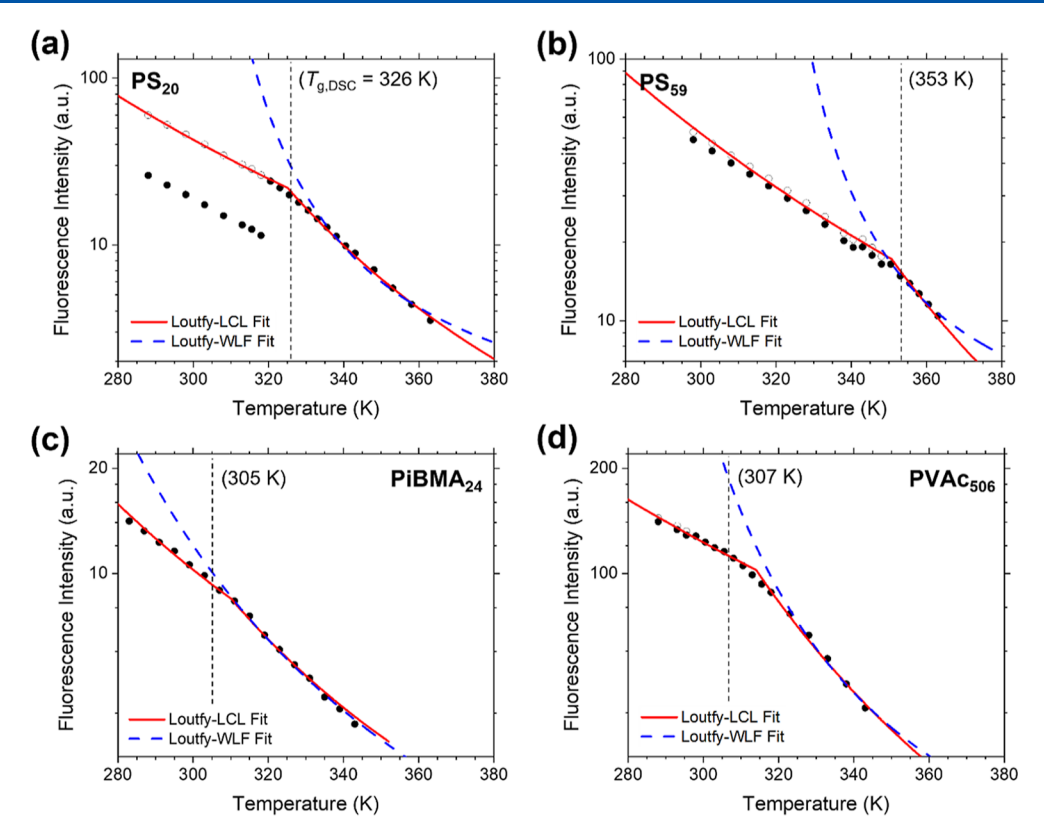


Figure 3. Fluorescence intensities of 0.01 wt % FCVJ in (a) PS₂₀, (b) PS₅₉, (c) PiBMA₂₄, and (d) PVAc₅₀₆ obtained during cooling at a rate of 0.5 K/min. The lower temperature portions of original data points (filled circles at $T < T_{\rm g}$) were shifted upward by a constant multiplication factor for correction for the loss of transmittance due to the formation of microcracks within the vitrified sample. The rescaled intensity data (open circles) were fit to the Loutfy equation (eq 1) on the basis of the LCL model-based total free volume definition (red solid line) or the WLF model-type excess free volume definition (blue dashed line) using $T_{\rm g}$ as the adjustable parameter. For comparison, the $T_{\rm g}$ values determined by DSC ($T_{\rm g,DSC}$) are also shown using (black) dotted vertical lines. Note that the PS₂₀ matrix exhibited a significantly lower peak intensity compared to the PS₅₉ matrix due to the light absorption by the trithiocarbonate PS end groups. The trithiocarbonate moiety has a molar absorptivity (ε) of approximately 10 L mol⁻¹ cm⁻¹ in the wavelength range of 475–490 nm.³⁵

showing significantly reduced intensities) was vertically shifted (by multiplication of a constant adjustment factor) to make the curve continuous across the temperature of crack formation (open circles in Figure 3).

As shown in Figure 3, in all cases the fluorescence intensity showed a discontinuous change in the slope of the $\log I$ vs. T graph at a temperature that is close to the $T_{\rm g}$ of the matrix polymer determined by differential scanning calorimetry (DSC) (" $T_{\rm g,DSC}$ ", indicated using dashed vertical lines in the figure). The I-T profiles were fitted to a model (derived from the Loutfy model (eq 1)) that accounts for free volume-dependent changes in non-radiative decay rate

$$\log I(T) \cong C' + x/f(T; T_g) \tag{2}$$

where C' and x are system-specific, temperature-independent parameters, and $f(T;T_{\rm g})$ is the fractional free volume which is a function of both the measurement temperature (T) and the glass transition temperature $(T_{\rm g})$ (as will be discussed further below); the derivation of eq 2 is shown in the Methods section. Here, x is the coupling parameter (discussed in the Introduction); 15,16 x=0 means no coupling, and x=1 means complete coupling between the rotor rotation and the monomeric friction. In the fitting analysis, C', x and $T_{\rm g}$ were used as adjustable parameters. The fractional free volume, $f(T;T_{\rm g})$ was estimated as a function of T using the two different definitions of free volume for comparison—(i) the LCL model-based "total" free volume $(V_{\rm ftot} \equiv V - V_{\rm hc})$, and

(ii) the conventional "excess" free volume $(V_{\rm f,exc} \equiv V - V_{\rm vib})$ used, for instance, in the WLF theory; see Figure 1 for graphical depiction of these definitions. The LCL model predicts that there exists a universal correlation between $f_{\rm g}$ and $T_{\rm g}$; $f_{\rm g}(T_{\rm g}) = aT_{\rm g} + b$ where $a = 3.31 \times 10^{-4}~{\rm K}^{-1}$ and $b = -1.49 \times 10^{-2}$ (a and b are universal constants). Thereafter, in the LCL model-based analysis, $f(T;T_{\rm g})$ is estimated as

$$f(T; T_g) = f_g(T_g) + \alpha_L(T - T_g) \text{ for } T > T_g$$
(3a)

$$f(T; T_{\rm g}) = f_{\rm g}(T_{\rm g}) + \alpha_{\rm G}(T - T_{\rm g}) \text{ for } T < T_{\rm g}$$
(3b)

where $\alpha_{\rm G}$ and $\alpha_{\rm L}$ are the thermal expansion coefficients of the polymer in the glass and liquid states, respectively (Table 1). In contrast, the conventional definition of the free volume $(V_{\rm f,exc} \equiv V - V_{\rm vib})$ gives³⁶

$$f(T; T_{\rm g}) = f_{\rm g} + (\alpha_{\rm L} - \alpha_{\rm G})(T - T_{\rm g}) \text{ for } T > T_{\rm g}$$
 (4a)

$$f(T; T_{g}) = f_{g} \text{ for } T < T_{g}$$

$$\tag{4b}$$

The WLF theory, which uses the conventional excess free volume $(V_{\rm f,exc})$, gives that $f_{\rm g}=(\alpha_{\rm L}-\alpha_{\rm G})[C_2-(T_{\rm r}-T_{\rm g})]$ where C_2 is the second WLF coefficient determined at a reference temperature of T_v or alternatively, $f_{\rm g}=(\alpha_{\rm L}-\alpha_{\rm G})C_2^{\rm g}$ when $T_{\rm r}=T_{\rm g}$ (here, $C_2^{\rm g}$ denotes the value of C_2 at $T_{\rm r}=T_{\rm g}$). The rotor fluorescence data shown in Figure 3 were fit to the Loutfy model (eq 2) using the two different free volume

definitions discussed above—(i) $V_{\rm f,tot}$ (eqs 3a and 3b, "Loutfy—LCL fit") vs. (ii) $V_{\rm f,exc}$ (eqs 4a and 4b, "Loutfy—WLF fit")—using C', x and $T_{\rm g}$ as fitting parameters; note in the "Loutfy—WLF fit" case, the data were fit only for $T > T_{\rm gr}$ because, as can be seen from eqs 4a and 4b (and eq 2), the conventional excess free volume definition predicts a constant value of f (and thus a constant value of f) at f0 and therefore, it fails to capture experimental data in the glassy region. The best-fit values of f1 and f2 for the four different homopolymers (obtained from the two different fitting methods) are given in Table 2.

As shown in Figure 3, the Loutfy model on the basis of the LCL model-based total free volume definition (V_{ftot}) (Loutfy-LCL fit) was able to precisely reproduce the FCVJ fluorescence intensity profiles over the entire temperature range covering both the glassy and liquid states, and the best-fit $T_{\rm g}$ values $(T_{
m g,LCL})$ were in good agreement with the values determined by DSC $(T_{g,DSC})$ (Table 2). As shown in the figure, the log I vs. T plots showed a slope break at T_g , and this feature was precisely captured by the model, because the model predicts that $|d(\log I)/dT|_g = \alpha(x/f_g^2)$ at T_g ; the limiting slope $(|d(\log I)/dT|_g)$ on the liquid side (at $T > T_g$) is steeper than that on the glass side (at $T < T_g$) because $\alpha_L > \alpha_G$. The values of the coupling parameters (x) were found to vary from polymer to polymer in the range x = 0.37 - 0.82, which suggests that x depends on the strength of the FCVJ-polymer interaction (further discussed later). To the contrary, for the reason discussed above, the Loutfy model on the basis of the WLF model-type excess free volume definition $(V_{\rm f,exc})$ (Loutfy-WLF fit) was only able to reproduce the liquidstate data, and the fitting produced significantly overestimated values of $T_{\rm g}$ ($T_{\rm g,WLF}$, Table 2). The values of the coupling parameters (x = 0.03-0.12) were also significantly lower than those obtained from the Loutfy–LCL fit procedure (x = 0.37– 0.82); note these x values obtained from the Loutfy-WLF fit are consistent with the values previously reported in the literature (x = 0.06-0.11). As graphically explained in Figure 1, the difference between the total free volume ($V_{
m f,tot}$ used in the Loutfy–LCL fit) and the excess free volume ($V_{\rm f,exc}\!$ used in the Loutfy–WLF fit) is the quantity called the vibrational free volume $(V_{\rm f,vib}=V_{\rm f,tot}-V_{\rm f,exc})^{20}$ This vibrational free volume is the space swept by (picosecond-scale) vibrational motion of the monomers within individual cages, and as illustrated in Figure 1, it expands with temperature regardless of whether T is greater or less than $T_{\rm g}^{20,37}$. The incorporation of this $V_{\rm f,vib}$ quantity in the definition of free volume $(V_{f,tot})$ is thus what enabled the Loutfy-LCL model to capture the temperaturedependent variation of the fluorescence intensity of FCVJ even at $T < T_g$ of the matrix polymer.

Timescales of PS Monomer Diffusion Versus FCVJ Rotor Rotation. In an effort to better understand why FCVJ probes changes in $V_{\rm f,tot}$ (instead of $V_{\rm f,exc}$), we computed the center-of-mass mean square displacements (MSD) of monomers ($\langle r^2 \rangle$) for PS₂₀ at three different temperatures, $T=460~{\rm K}$ (> $T_{\rm g}$), 320 K ($\cong T_{\rm g}$), and 200 K (< $T_{\rm g}$), by atomistic MD simulations. The results are presented in Figure 4c. As shown in the figure, at 460 K, the monomer movement at short times (< \sim 1 ps) was purely diffusive (that is, $\langle r^2 \rangle \sim t$), whereas at long times ($\gg \sim$ 100 ps) the Rouse sub-diffusive behavior was observed ($\langle r^2 \rangle \sim t^{0.5}$); at intermediate times, the MSD exhibited a plateau that is characteristic of monomers "caged" by neighboring monomers (Figure 4a). This result is in quantitative agreement with previous results. ³⁸ At 320 and 200

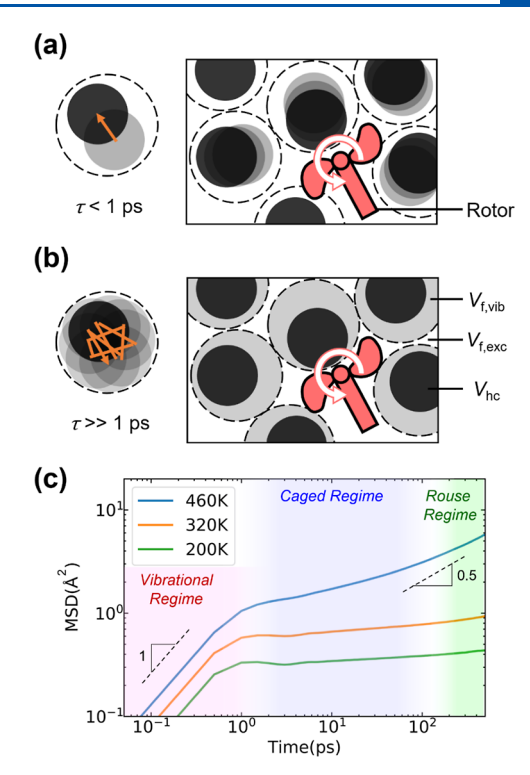


Figure 4. (a,b) Schematic illustrations explaining how the relevant free volume quantity is changing, depending on the speed (time scale) of a rotor's rotational motion. The microscopic definitions of the hard-core (van der Waals) volume ($V_{\rm hc}$), the vibrational free volume $(V_{
m f,vib})$, and the excess free volume $(V_{
m f,exc})$ are also graphically described. (a) The monomers (black circles) are in constant vibration and have a mean free time of ~ 1 ps (as shown in (c)), which corresponds to the time it takes for the center of mass of a monomer to move around by diffusion before it encounters the confinement boundary (orange arrow). If the intrinsic rotation time of a rotor ($\tau \equiv$ $1/k_{\rm rot}^{0}$ is comparable to or shorter than this timescale (≈ 1 ps), the rotation of the rotor (pink) would not be hindered by the vibration (diffusion) of the monomers; only the hard-core volumes (not the vibrational volumes) of the surrounding monomers contribute to the friction against the rotation of the rotor. (b) If the rotor rotation is much slower than the monomer vibration ($\tau \gg 1$ ps), the rotor rotation would be hindered by the monomer vibration; the entire occupied volumes (i.e., the vibrational volumes defined in Figure 1) of the surrounding monomers produce friction against the rotor. (c) MSDs of the monomer centers of mass were calculated by atomistic MD simulation for PS_{20} at three different temperatures (both above and below $T_{\rm g}$). Color shades show different regimes of dynamic behavior: vibrational/diffusive (red), caged (blue), and Rouse/subdiffusive (green).

K, the Rouse regime could not be reached within the simulation time (\sim 0.5 ns). However, the vibrational mean free time (i.e., the upper time limit for the early diffusive behavior, \sim 1 ps) was found to be identical for all three temperatures. In the literature, it is known that the intrinsic timescale of rotor rotation is of the order of a picosecond (or less); the non-radiative decay of DCVJ, which has the same julolidine headgroup as FCVJ (Figure 2a), for instance, was measured to occur within a timescale of \sim 1 ps in low-viscosity media. ^{39,40} Therefore, it is reasonable to expect that the local vibration of the monomers does not actually cause much friction against the rotation of FCVJ (because the FCVJ rotation is almost as fast as the monomer vibration) and, therefore, the relevant free volume quantity that is being

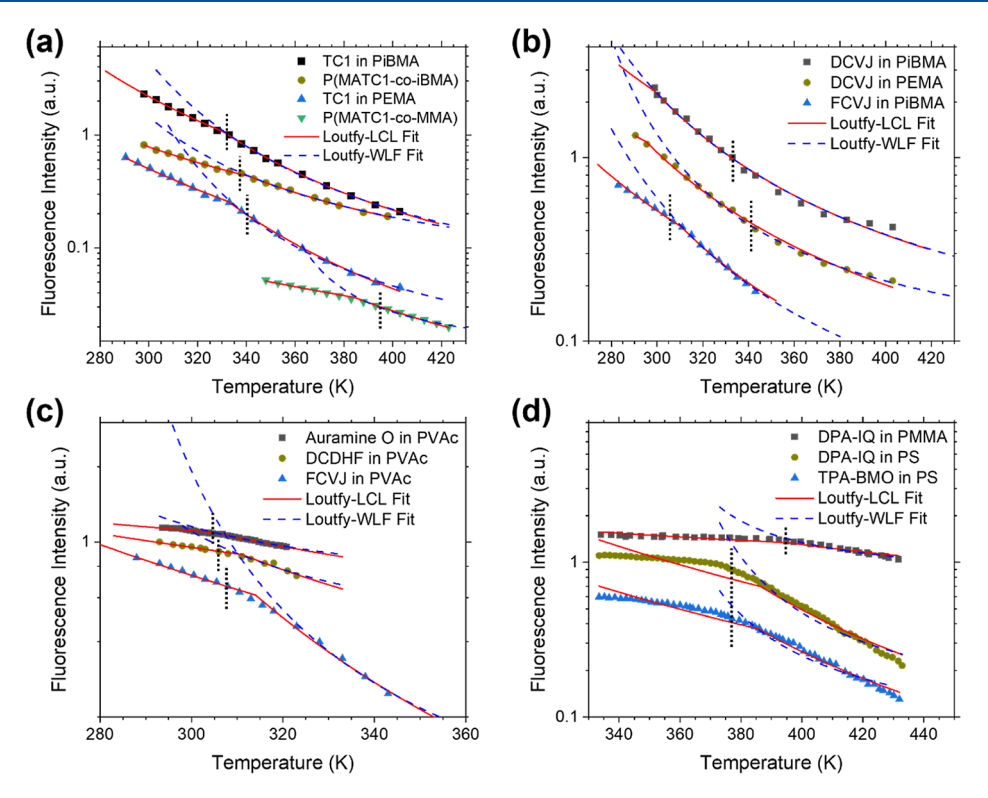


Figure 5. Fitting of rotor fluorescence data from the literature to the Loutfy equation on the basis of the LCL model-based total free volume definition (red solid lines) or WLF model-type free volume definition (blue dashed lines). T_g values determined by DSC are shown using dotted vertical lines (black). The intensity profiles were vertically shifted for clarity. (a) TC1-doped PiBMA (a film of thickness > 2 μ m); ¹⁵ TC1-doped PEMA (a film of thickness > 2 μ m); ¹⁵ a copolymer of MATC1 and iBMA (a film of thickness > 2 μ m); ¹⁵ a copolymer of MATC1 and MMA (a film of thickness > 0.2 μ m); ¹⁶ (b) DCVJ-doped PiBMA (a film of thickness > 2 μ m); ¹⁵ DCVJ-doped PEMA (a film of thickness > 2 μ m); ¹⁵ FCVJ-doped PiBMA (bulk, this study). (c) Auramine O-doped PVAc (a cylindrical specimen with unknown dimensions); ⁶ DCDHF-doped (a film of thickness > 60 μ m); ⁹ FCVJ-doped PVAc (bulk, this study). (d) DPA-IQ-doped PMMA (a film of unknown thickness); ⁴⁴ DPA-IQ-doped PS (a film of unknown thickness); ⁴⁴ TPA-BMO-doped PS (a film of unknown thickness).

Table 3. Results of the Fitting of Molecular Rotor Fluorescence Data from the Literature to the Loutfy Model on the Basis of the Two Different Free Volume Definitions (LCL Model-based $V_{\text{f,tot}}$ vs WLF Model-type $V_{\text{f,exc}}$)

						Loutfy-LCL fit			Loutfy-WLF fit		
rotor/matrix	$T_{\rm g,DSC}$ (K)	$\alpha_{\rm G}~(10^{-4}~{\rm K}^{-1})$	$\alpha_{\rm L} \ (10^{-4} \ { m K}^{-1})$	C_2^g (K)	$f_{\rm g,WLF}$	T _{g,LCL} (K)	х	C'	T _{g,WLF} (K)	х	C'
TC1/PiBMA ¹⁵	332	3.8^{32}	6.1 ³²		0.030	331	0.49	-5.10	332	0.14	-4.49
TC1/PEMA ¹⁵	340	2.75^{32}	5.4 ³²	90.3^{31}	0.024	333	0.61	0.00	330	0.10	-4.12
$P(MATC1-co-iBMA)^{15}$	337	3.8^{32}	6.1 ³²		0.030	341	0.30	0.04	337	0.08	-2.79
$P(MATC1-co-MMA)^{18}$	395	2.15^{32}	4.6 ³²	52.4 ³¹	0.013	384	0.50	-3.87	387	0.02	-0.74
DCVJ/PiBMA ¹⁵	332	3.8^{32}	6.1 ³²		0.030	299	0.36	-3.43	298	0.13	-3.35
DCVJ/PEMA ¹⁵	340	2.75^{32}	5.4 ³²	90.3^{31}	0.024	295	0.37	0.03	318	0.06	-2.19
auramine O/PVAc ⁶	305	2.1 ³³	5.2 ³³	65.7^{34}	0.026	305	0.12	93.49	305	0.02	5.22
DCDHF/PVAc ⁹	306	2.1 ³³	5.2 ³³	65.7^{34}	0.026	312	0.23	0.07	311	0.03	-1.22
DPA-IQ/PMMA ⁴⁴	394	2.15^{32}	4.6 ³²	52.4 ³¹	0.013	396	0.16	0.22	394	0.01	-0.73
DPA-IQ/PS ⁴⁴	376	2.6^{20}	6.2^{20}	57.1 ³¹	0.016	387	0.58	0.00	381	0.04	-2.65
TPA-BMO/PS ⁴⁴	376	2.6^{20}	6.2 ²⁰	57.1 ³¹	0.016	386	0.53	0.06	376	0.04	-2.36

probed by FCVJ is the total free volume $(V_{\rm f,tot} = V_{\rm f,exc} + V_{\rm f,vib})$, instead of the excess free volume $(V_{\rm f,exc})$ (Figure 4b). Note, on the other hand, the monomer relaxation ("Rouse") time, defined as the time it takes for a monomer to travel a distance comparable to its size $(\langle r^2 \rangle^{1/2} \approx b \cong 0.7$ nm for a PS monomer unit), was much greater than the simulation time (\sim 0.5 ns) even at 460 K (Figure 4c), and it further increased rapidly with decreasing T, as also shown in other previous studies. ^{41,42} At temperatures close to the glass transition, the monomer relaxation times of polymers are known to be on the order of micro- to milliseconds (at the minimum). ⁴³ Therefore, the

monomer relaxation must be controlled by the friction from the vibrational volume $(V_{\rm vib})$ (not by the friction from the hard-core volume $(V_{\rm hc})$); in this case, the relevant free volume is the conventional, excess free volume $(V_{\rm f,exc})$.

Other Rotor/Polymer Combinations. The same analysis was performed on data available in the literature for other rotor/polymer combinations; the chemical structures of the molecular rotors studied are presented in Figure 2a. Note, as shown in Figure 2a, DCVJ has the same julolidine headgroup as FCVJ but no hydrocarbon tail, and TC1 also has a similarly sized headgroup structure. The results of the analysis are

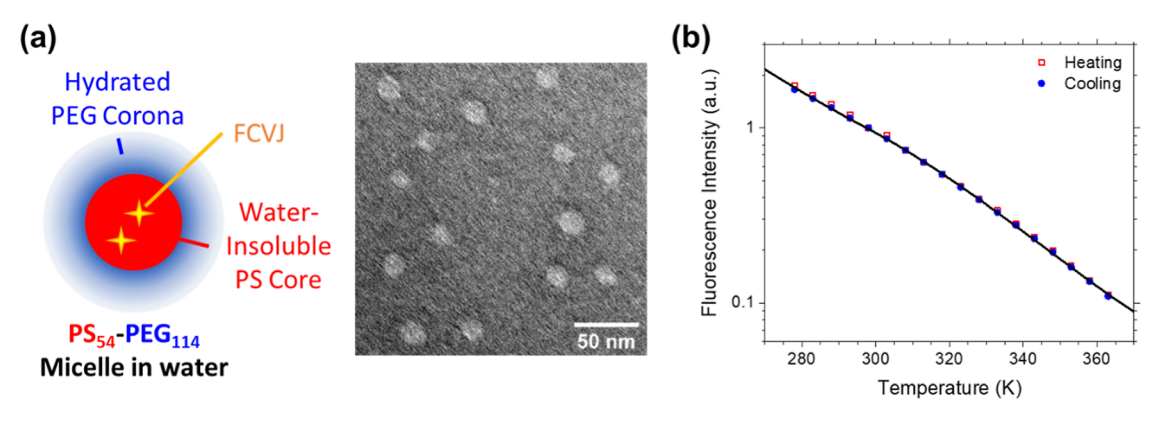


Figure 6. Determination of the $T_{\rm g}$ of the cores of PS-PEG micelles in water via FCVJ fluorescence intensity measurement. (a) Schematic illustration of an FCVJ-loaded PS₅₄-PEG₁₁₄ micelle, and a representative, dry-state TEM image of spherical PS₅₄-PEG₁₁₄ micelles having an average core diameter of 20 nm. (b) Fluorescence intensities from an aqueous solution containing 0.5 wt % FCVJ-loaded PS₅₄-PEG₁₁₄ micelles in water measured as a function of temperature during a heating and cooling cycle in the range of 278–363 K at a heating/cooling rate of 0.5 K/min. The data obtained during cooling were fit to the Loutfy model on the basis of the LCL model-based total free volume definition assuming a constant distribution of $T_{\rm g}$ between 298 and 357 K; the fit is shown using the solid line.

presented in Figure 5 and Table 3. As shown in Figure 5a, the Loutfy-LCL model provided excellent fits to I-T data from TC1-doped PiBMA, TC1-doped poly(ethyl methacrylate) (PEMA), 15 MATC1 copolymerized with iso-butyl methacrylate (P(MATC1-co-iBMA)), 15 and MATC1 copolymerized with methyl methacrylate (P(MATC1-co-MMA))¹⁸ over the entire range of T examined covering both the liquid and glassy states. The data in the liquid region were also fit well with the Loutfy-WLF model (Figure 5a). As shown in Table 3, the fit results, that is, the resulting $T_{\rm g,LCL}$ and $T_{\rm g,WLF}$ values, agreed well with each other and also with the $T_{\rm g,DSC}$ values reported in the respective references. However, as shown in Figure 5b and Table 3, for the DCVJ-doped systems, 15 both the Loutfy-LCL and Loutfy-WLF fit methods did not produce T_g values (i.e., $T_{g,LCL}$ and $T_{g,WLF}$, respectively) that are in agreement with DSC data. We note that TC1, MATC1 and DCVJ have the same dicyanomethylene tail group moieties, but they differ in their aniline-based headgroup structures, which appears to have caused different coupling behaviors. It is not currently understood how the headgroup chemistry influences the rotor's fluorescence behavior. However, one possible explanation for the difference between TC1 and DCVI is that the hydroxyl groups on TC1 form hydrogen bonds with the ester carbonyl groups on the methacrylate units of the polymers, which must have caused increased coupling between the rotor and the polymer matrix.

Figure 5b displays a comparison between DCVJ and FCVJ; these results elucidate the effect of the rotor's tail-group structure on the sensitivity of the rotor probe to the thermomechanical state of the polymer matrix. As shown in the figure, FCVJ was able to precisely determine the T_g of the matrix polymer, whereas DCVJ was unable to do so. We believe that the long farnesyl tail of FCVI enabled strong coupling between the internal rotation (twisting) of the rotor molecules and the thermal fluctuations of the polymer segments, while in the DCVJ case the dicyanomethylene tail was too small to produce such an effect. As shown in Figure 5c, other similar rotors with relatively small tail groups (such as auramine O and DCDHF (Figure 2a) were also unable to precisely detect the $T_{\rm g}$ of the matrix polymer. As summarized in Table 3, the values of the coupling parameters for these short-tail rotors (DCVJ, auramine O, and DCDHF) were consistently lower (x = 0.12-0.37, obtained from the Loutfy-

LCL fit) relative to the values obtained for FCVJ using the same fitting procedure (x = 0.37-0.82, Table 3). We suspect that the tail groups of the DCVJ, auramine O, and DCDHF molecules are not larger, perhaps smaller, than the cavity within the polymer matrix ($\approx V_{\rm f,exc}(T_{\rm g})$, Figure 1), and thus their internal rotation is not hindered to a measurable extent by adjacent monomers. This interpretation is supported by data available in the literature. The average cavity (hole) volumes of the polymer materials discussed in this article, obtained from positron annihilation lifetime spectroscopy at or near 25 °C, are as follows: 98 Å³ for PS (190 kDa),⁴⁵ 116 Å³ for PMMA (15 kDa),⁴⁵ 90 Å³ for PVAc (molecular weight unspecified), 46 79 Å3 for PMMA (86 kDa), 47 and 88 Å3 for PEMA (154 kDa).⁴⁷ Most of the common matrices have average hole volumes close to 100 Å³, corresponding to a hole radius of 2.9 Å. However, it should be noted that this determination was based on the measured ortho-positronium lifetime using the Tao model for a spherical potential well.⁴⁶ It is possible that the effective dimension of the cavity in the matrix is smaller than the "hole diameter" (5.8 Å), as the realistic cavity structure resembles a percolated channel rather than an isolated sphere. The main rotating part in DCVI and DCDHF, the dicyanomethylene tail group, extends 3.1 Å from the rotating axis to the tip of the edge; the size of the dicyanomethylene group is at most comparable to the cavity in those polymers. In contrast, the rotating part in FCVJ, the farnesyl acetate tail group, has a radius of gyration of 3.7 Å, as calculated from our MD simulation; the size of the farnesyl acetate group is indeed slightly larger than the "hole radius", leading to friction when the probes attempt to rotate. Therefore, this larger tail group size confers greater sensitivity to FCVJ compared to the other probes. A study using molecular rotors with systematically varying tail group lengths would allow us to quantitatively determine the cavity size of a matrix polymer.

Interestingly, neither of the two analysis methods (Loutfy–LCL and Loutfy–WLF fit procedures) were able to quantitatively describe the I-T profiles of DPA-IQ in PS and PMMA, ⁴⁴ and TPA-BMO in PS⁴⁴ (Figure 5d; also, see Table 3 for the x values); in ref 44, these rotors were described as "aggregation-induced-emission luminogens (AIEgens)". As shown in Figure 5d, in these AIEgen cases, the I-T profiles were nearly flat at $T < T_g$. As shown in Figure 2a, both DPA-IQ

ı

and TPA-BMO have a triphenylamine moiety, and they undergo non-radiative decay via the rotation of one of the phenyl rings. For a similar triphenylamine-based rotor, DPAP, the rate constant for non-radiative decay is known to be $k_{\rm nr}\cong$ 0.063 ns⁻¹ whereas the rate constant for radiative decay is known to be $k_r \cong 0.019 \text{ ns}^{-1}$, in PMMA (molecular weight unknown) at room temperature (i.e., $k_{\rm r}/k_{\rm nr} \cong 0.30$).⁴⁸ In this case, the Loutfy's model (eq 1) is not strictly applicable because the $k_{\rm nr} \gg k_{\rm r}$ condition is not satisfied. The relatively slow non-radiative decay rate of DPAP is thought to be due to its small driving energy for internal rotation; the driving energy for rotation of DPAP is known to be 5-8 kJ/mol (equivalent to 2–3 k_BT per molecule at 298 K where k_B is the Boltzmann constant).⁴⁸ Depending on the polymer type and temperature, the rotor's non-radiative decay rate can even become slower than its radiative decay rate $(k_r > k_{nr})$, which would lead to a saturation of the fluorescence quantum yield ($\Phi \cong 1$ as expected from eq 1) and thus a flat I-T profile. In analogy, the DPA-IQ and TPA-BMO AIEgens are expected to have similar levels of rotational energies and non-radiative decay rates smaller rotational energies and slower non-radiative decay rates than for other p-substituted aniline rotors (such as the ones shown in Figure 2a). We suspect this was the reason why the measured fluorescence profiles of the AIEgens showed plateaus at low temperatures ($< T_o$) and overall could not be described well using the free volume models.

Fluorescence from FCVJ-Loaded PS-PEG Micelles in Water. We further investigated whether FCVJ can be used to determine the $T_{\rm g}$ of nanoconfined polymers. Specifically, we were interested in measuring polymer micelle core $T_{\rm g}$ in aqueous solution because $T_{\rm g}$ is an important factor contributing to the performance of polymer micelles, for instance, in lung surfactant therapy 49-51 and controlled drug release⁵² applications. FCVJ was loaded within the hydrophobic PS core domain of spherical micelles (having a core diameter of 20 nm) formed in water by PS54-PEG114 (Figure 6a). This PS₅₄-PEG₁₁₄ diblock copolymer was synthesized by RAFT (from a monomethoxy monohydroxy PEG precursor purchased from Sigma-Aldrich). The molecular characteristics of PS₅₄-PEG₁₁₄ are summarized in Table 1. FCVJ was loaded into the micelle via solvent exchange from acetone (the initial cosolvent) with water (the final counter-solvent), and the FCVJ loading ratio was 0.1 wt % relative to the combined mass of PS and FCVJ. FCVJ-loaded PS_{54} -PEG₁₁₄ micelles were prepared at a concentration of 0.5 wt % in Milli-Q water for fluorescence measurements; this concentration was chosen because of its relevance to a typical concentration used in pharmaceutical particle formulations. 49,50

As shown in Figure 6b, the micelle sample showed a typical trend of increasing fluorescence intensity with decreasing temperature similarly to what was observed in bulk homopolymers. However, unlike the bulk situation, the micelle data could not fit well with the Loutfy–LCL free volume model. The change in the slope of the log I vs. T curve was more gradual (it occurred over a range of temperature from ~ 300 to ~ 350 K), and a single $T_{\rm g}$ value could not be determined, which suggests that there is a finite distribution of micelle core $T_{\rm g}$ values. We believe that the physically doped FCVJ molecules are likely randomly distributed within the micelle core domain, and they thus experience different freevolume environments depending on the distance from the confining interface (i.e., the micelle core surface in our case). Significant for the confining interface (i.e., the micelle fluorescence data shown

in Figure 6b, the Loutfy-LCL model was convoluted with a distribution function for the $T_{\rm g}$ values. For simplicity, we assumed a constant (flat) distribution of T_g between two limits $(T_{g,min} \text{ and } T_{g,max})$, as described in the Methods section; therefore, in this analysis, four parameters ($T_{
m g,min}$, $T_{
m g,max}$, x and C') were used as fitting variables. The fit result is displayed in Figure 6b (solid line), and the best-fit parameters are presented in Table 2. As can be seen from the figure, the fit quality was great. The value of the coupling parameter for the PS54- PEG_{114} micelles (x = 0.73) was quite comparable to that for the bulk PS_{59} (x=0.76). The $T_{g,min}$ and $T_{g,max}$ values were found to be 298 and 357 K, respectively. The mean micelle core $T_{\rm g}$ (328 K) was about 25 K lower that the bulk $T_{\rm g}$ of a comparably sized PS (353 K for PS $_{59}$). The width of the $T_{\rm g}$ distribution was quite large $(T_{g,max} - T_{g,min} = 59 \text{ K})$ because of the small size of the micelle core domain ($D_c \cong 20$ nm). All these results are in reasonable agreement with previously reported data obtained by DSC and pyrene fluorescence measurements for PS nanoparticles dispersed in water.⁵⁴⁻⁵⁷ For PS nanoparticles of ~20 nm diameter suspended in water, the degrees of nanoconfinement-induced T_g depression were found to vary in the range of 5-70 K depending on the type of surfactant used and the surface coverage of the surfactant. S In general, the local T_g of a nanoconfined polymer is known to change with distance from the confining interface. 58,59 In the present study, we did not attempt to determine the exact form of the T_g distribution within the micelle core domain; as mentioned above, a step function was used as a convenient approximation. A further study would be needed to delve into this problem, for instance, using the method of position specifically labeling subsets of PS chains with FCVJ.

Additional Discussions. Previous data available in the literature have demonstrated that the fluorescence behavior of molecular rotors is closely related to the free volume properties of polymer matrices, 3,6,9,15,16 and therefore molecular rotors are useful for measuring local $T_{\rm g}$ values and probing sub-glass relaxation processes (such as physical aging). ^{6–8,15,16,18,19,60} An analysis of our own data and also previous data in the literature now allows us to define key required characteristics of molecular rotors for use in free volume measurements as follows. Firstly, the non-radiative relaxation (i.e., internal rotation) of the molecular rotor should be inherently much faster than the radiative relaxation $(k_{\rm nr} \gg k_{\rm r})$ to avoid saturation of the fluorescence quantum yield ($\Phi \equiv k_{\rm r}/(k_{\rm r} +$ $k_{\rm nr}$)), particularly, in polymers near glass transition; otherwise, no measurable changes in fluorescence intensity with temperature will be detected. In this regard, julolidine-based rotors are promising, because their k_r values ($\approx 0.3 \text{ ns}^{-1}$) are about 3 orders of magnitude smaller than their $k_{\rm nr}$ values ($\approx 0.1-0.9$ ps⁻¹) in low-viscosity media,³⁹ which ensures that even in high-viscosity media the $k_{\rm nr} > k_{\rm r}$ condition still holds. The second is regarding the type of free volume to be measured. As just discussed above, the ideal rate of non-radiative decay (k_{nr}) is of the order of $\sim 1 \text{ ps}^{-1}$ for a molecular rotor to be used for T_g determination. As discussed in a previous subsection, this non-radiative decay rate is also appropriate from the standpoint of detecting changes in the total free volume $(V_{\rm ftot})$ (rather than the conventional excess free volume $(V_{\rm f,exc})$), because the rate of local monomer diffusion (vibration) is roughly of the same order. Interestingly, the $T_{\rm g}$ values determined using a rotor that satisfies this requirement (namely, FCVJ) well agree with the T_g values determined by DSC which is the most common T_g measurement technique.

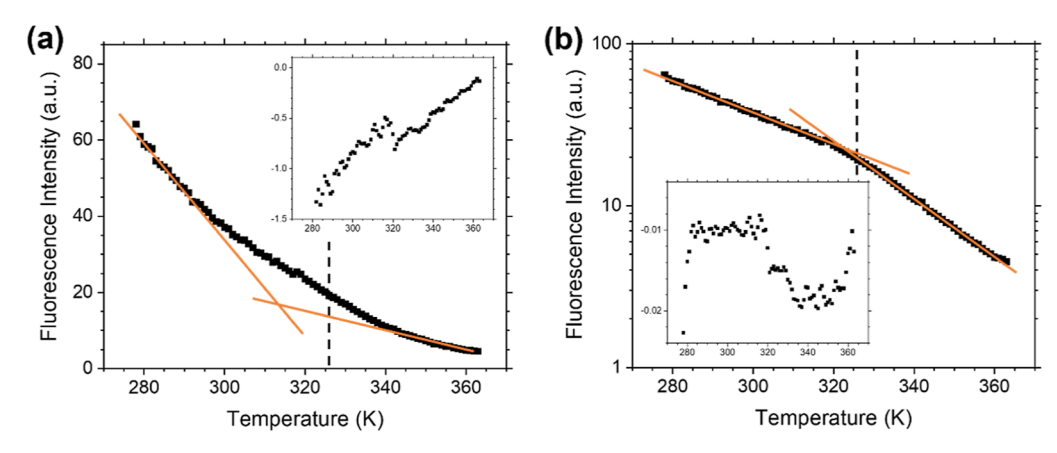


Figure 7. Demonstration of the $T_{\rm g}$ determination by the bilinear slope analysis procedure performed on the (a) linear—linear and (b) log-linear plots of fluorescence intensity (I) vs. temperature (T) for FCVJ-doped PS₂₀. The $T_{\rm g}$ is defined as the temperature of intersection of the two extrapolating linear expansion lines from above and below the glass transition range (orange solid lines). For comparison, the value of $T_{\rm g,DSC}$ (=326 K) is marked with the black vertical line. Insets are (a) dI/dT vs. T and (b) d(log I)/dT) vs. T plots; it is clearly visible that the log I vs. T plot has constant slopes in both the liquid ($T > T_{\rm g}$) and glassy ($T < T_{\rm g}$) regions and a slope break around $T_{\rm g}$.

Lastly, for precise determination of $T_{\rm g}$, the rotational movement of a molecular rotor must be strongly coupled with the dynamics of the matrix polymer chains. We found that this rotor-matrix coupling can be enhanced using a rotor with a longer tail group and also with a stronger interaction with the matrix polymer. To elucidate the effects of molecular rotors' size/interaction characteristics on their $T_{\rm g}$ measurement performance, further systematic studies are warranted.

We were encouraged by our results, especially, the successful fitting of FCVJ data with the Loutfy–LCL model demonstrated in Figure 3, to further test whether a more recent theory, named the Cooperative Free Volume (CFV) rate model, can fit the data even better. In the CFV model, to account for the difference in the relative sensitivity of a material's dynamics to changes in T vs. changes in V, the original Doolittle relation ($\log \eta \sim 1/f$) is modified to a form, $\log \eta$ ($\sim \log \tau$) $\sim (1/f)$ (T^*/T) where τ is the structural (α) relaxation time, and T^* and b are material-specific dynamic parameters; for instance, for PVAc, $T^* = 421$ K, and b = 3.90. In the CFV model, the additional temperature-dependent term, that is, (T^*/T), was introduced in order to properly model segmental α relaxation times for various polymers. Based on this CFV formalism, the Loutfy equation (eq 1) can also be modified as

$$\Phi \cong (k_r/k_{\text{rot}}^0) \exp[(xf_0/f)(T^*/T)^b]$$
(5)

However, we found that, unlike the Loutfy–LCL model, this Loutfy–CFV model was unable to quantitatively fit, for instance, FCVJ/PVAc fluorescence data ($T_{\rm g}$, x and C' used as adjustable parameters, results not displayed). This result, conversely, suggests that the non-radiative relaxation (rotation) of FCVJ requires a smaller amount of free volume than required for the polymer matrix's segmental α relaxation; the rotation of FCVJ does not require the polymer segments to make large rearrangements.

The $T_{\rm g}$ determination by the Loutfy–LCL analysis requires information about the thermal expansion coefficients ($\alpha_{\rm G}$ and $\alpha_{\rm L}$). As a simpler approximation, we suggest a bilinear slope analysis method using log I vs. T plots; this procedure does not require a priori knowledge of the values of $\alpha_{\rm G}$ and $\alpha_{\rm L}$. The rationale for this method is as follows. As can be shown from eq 2, the slope of the log I vs. T plot is given as (i) $d(\log I)/dT$

 $= -\alpha_G(x/f^2)$ at $T < T_g$, and (ii) $d(\log I)/dT = -\alpha_L(x/f^2)$ at T $> T_g$; here, f is a function of T and changes discontinuously across T_g (Figure 1), and the glassy and liquid states have different values of thermal expansion coefficient ($lpha_{
m G}$ and $lpha_{
m L}$) respectively). Therefore, the slope of the log I vs. T plot must also change discontinuously at the glass transition point. Interestingly, however, in the literature it is more common to use I vs. T plots (instead of log I vs. T plots) for bilinear $T_{\rm g}$ analysis, 6,9,18,19,44 but we have not been able to come up with a clear mathematical justification for this approach. Figure 7 compares the I vs. T versus log I vs. T plots for FCVJ-doped PS₂₀ (a separate measurement conducted using the same sample as shown in Figure 3a). As shown in Figure 7a, the bilinear analysis using the I vs. T plot did not give an accurate estimate for the $T_{\rm g}$ of the polymer, because the slope of the curve changed rather gradually over a large range of T; see also the inset of Figure 7a for a corresponding dI/dT vs. T plot. To the contrary, the bilinear limiting-slope analysis of the log *I* vs. T curve led to an accurate determination of T_g (Figure 7b); as shown in the inset of Figure 7b, $d(\log I)/d\tilde{T}$ showed a step change at $T_{\rm g}$, and the resulting $T_{\rm g}$ estimate $(T_{\rm g} = 326 \text{ K})$ agreed well with the Loutfy-LCL analysis ($T_g = 325$ K) within less than 1 K. In the PS₅₄-PEG₁₁₄ micelle case, because of the distribution of T_g inside the core domain, $d(\log I)/dT$ did not show any discontinuous change at any particular temperature; as shown in Figure S3, the slope of the log I vs. T curve rather continuously decreased over the entire range of T examined.

CONCLUSION

Fluorescent molecular rotors are known to be able to probe changes in the matrix free volume with temperature. However, it has not been clear what exactly is the free volume quantity that molecular rotors are measuring. From the analysis of data obtained from various combinations of different types of molecular rotors and matrix polymers (including both our own data and also data from the literature), we found that the relevant free volume quantity that is probed by molecular rotors is the total free volume $(V_{\rm f,tot} = V_{\rm f,exc} + V_{\rm f,vib})$ (instead of the excess free volume $(V_{\rm f,exc})$) of the matrix polymer. Notably, the Loutfy rotor fluorescence model on the basis of the LCL model-based $V_{\rm f,tot}$ definition ("Loutfy–LCL model") was able to precisely reproduce the fluorescence intensity profiles of

FCVJ molecular rotors doped in various different types of polymers (PS, PiBMA and PVAc) over wide ranges of temperature covering both the glassy and liquid states of the polymers, and the best-fit $T_{\rm g}$ values $(T_{\rm g,LCL})$ were in good agreement with the values determined by DSC $(T_{\rm g,DSC})$. The same method was also applied to analyze fluorescence data from FCVJ-loaded PS-PEG micelles in water and allowed us to determine the distribution of local T_g values within the micelle core domain. A comparison among different types of rotors led us to conclude that a suitable rotor for T_{α} measurement must possess a relatively fast non-radiative decay rate (faster than its radiative decay rate) (e.g., FCVJ), and its rotational movement must be strongly coupled with the dynamics of the matrix polymer chains (for instance, due to a large tail-group size (e.g., FCVJ) and/or via formation of hydrogen bonds with the matrix polymers (e.g., TC1)). We found that a bilinear limiting-slope analysis procedure could also be used (as a convenient approximation to the Loutfy-LCL fit method) to determine the $T_{\rm g}$ of a polymer with a reasonable accuracy, but the bilinear analysis must be performed using data in the form of log I vs. T plots (instead of I vs. T plots), because the fluorescence intensity (I) follows a Doolittle-type exponential dependence on the thermal expansion coefficient ($\alpha_{\rm L}$ and $\alpha_{\rm G}$) as suggested by the Loutfy-LCL model.

METHODS

Synthesis of FCVJ. The fluorescent molecular rotor used in this study, FCVJ, was synthesized using the procedure reported in a previous publication (Figure S4a).²¹ Briefly, trans,trans-farnesol (5.0 mmol, Sigma-Aldrich) and cyanoacetic acid (CA, 5.0 mmol, Sigma-Aldrich) were first conjugated via the Steglich esterification in the presence of N-dicyclohexylcarbodiimide (DCC, 5.0 mmol, Sigma-Aldrich) and 4-dimethylaminopyridine (DMAP, 0.5 mmol, Sigma-Aldrich) dissolved in anhydrous dichloromethane (10 mL) to produce farnesyl cyanoacetic ester. ⁶³ The ester product was isolated from the reaction mixture by column chromatography (absorbent = silica gel, eluent = a 30:70 by volume mixture of ethyl ether and hexane) and dried under vacuum. The results of thin-layer chromatography (TLC) with silica gel and a 30:70 ethyl ether/ hexane eluent were: R_f (retention/retardation factor) = 0.17 (CA), 0.30 (farnesol), 0.60 (DCC), 0.02 (DMAP), and 0.63 (farnesyl ester). The purity of the isolated farnesyl ester was measured by ¹H NMR to be ~100 mol %.

Next, 9-julolidine aldehyde (JA, 1.3 mmol, Sigma-Aldrich) was conjugated to the farnesyl ester (2.0 mmol) through the aldol condensation in the presence of triethylamine (2.5 mmol; Sigma-Aldrich) dissolved in anhydrous tetrahydrofuran (5 mL) to produce FCVJ. The FCVJ product was further isolated from the reaction mixture by column chromatography (silica gel, 30:70 ethyl ether/ hexane) and dried under vacuum. The results of TLC with silica gel and a 30:70 ethyl ether/hexane eluent were: $R_f = 0.37$ (JA), and 0.34 (FCVJ). The purity of the isolated FCVJ was measured by ¹H NMR to be 94 mol %. The major impurity was JA (Figure S4b) which does not influence the $T_{\rm g}$ measurement because its fluorescence is not sensitive to the local viscosity environment. Further, under excitation at 475-490 nm, the fluorescence emission of JA at an emission wavelength of 520 nm was negligible relative to that of FCVJ (Figure S4c). Therefore, the residual amount of JA must not affect our FCVJbased T_g measurements.

Synthesis of Polymers. PS and PiBMA homopolymer and poly(styrene-block-ethylene glycol) (PS-PEG) deblock copolymer samples used in this study were synthesized by RAFT using the procedure described in our previous publication.⁴⁹ For the synthesis of the PS homopolymers, styrene (monomer, Sigma-Aldrich, purified with activated alumina (to remove free radical inhibitors)), azobisisobutyronitrile (AIBN, initiator, Sigma-Aldrich, used as

received), and 4-cyano-4-[(dodecylsulfanylthiocarbonyl)sulfanyl] pentanoic acid (CDSP, RAFT agent, Sigma-Aldrich, used as received) were initially dissolved in anhydrous 1,4-dioxane (Sigma-Aldrich) in an $\rm N_2$ -filled flask. The temperature was then raised to 75 °C, and the polymerization was run at that temperature for 20 h. The reaction was terminated by exposure to air and subsequent precipitation of the polymer content in methanol. The polymer product was isolated from the reaction mixture by precipitation in cold methanol (4 °C) 3 times and dried under vacuum overnight. The PiBMA homopolymer was synthesized in a similar manner.

For the synthesis of the PS-PEG diblock copolymer, monomethoxy monohydroxy PEG (5 kDa, Sigma-Aldrich) was first converted to "PEG-CDSP" by Steglich esterification with CDSP. 49,63 The PEG-CDSP product was purified by dissolving in dichloromethane and precipitating from cold hexane 3 times. Styrene (monomer), AIBN (initiator), and PEG-CDSP (RAFT agent) were dissolved in 1,4-dioxane, and the RAFT polymerization was run at 75 °C for 20 h. The PS-PEG product was precipitated in cold hexane (4 °C) 3 times and dried under vacuum overnight.

Characterizations of Polymers. The number-average degrees of polymerization (DP_n) of the PS, PiBMA, and PS-PEG samples were characterized by ¹H NMR spectroscopy using CD₂Cl₂ (for PS and PS-PEG) and CDCl₃ (for PiBMA) as the NMR solvents; the DP_n of PS was calculated from the area ratio of the peaks corresponding to the phenyl protons in the styrene units (7.5-6.0 ppm) and the methylene protons (-CH₂-) adjacent to the trithiocarbonate group at the chain end (3.26-3.05 ppm) (Figure S5); the DP_n of PiBMA was calculated from the area ratio of the peaks corresponding to the ether protons in the isobutyl methacrylate units (3.8-3.5 ppm) and the methylene protons (-CH₂-) adjacent to the trithiocarbonate group at the chain end (3.3-3.05 ppm) (Figure S6); the DP_n of the PS block of PS-PEG was calculated from the area ratio between the peaks corresponding to the phenyl protons in the styrene units (7.5-6.0 ppm) and the ether protons in the ethylene glycol units (4.14-3.30 ppm) (Figure S5). The overall molecular weight polydispersity indices (M_w/M_n) of these polymers were measured by GPC against PS standards. GPC measurements were performed using THF as the eluent at 35 °C and a refractive index detector (Figure S7). The glass transition temperatures (T_g) of polymers were determined by DSC; the samples were initially annealed at 433 K for 30 min and then subjected to two cycles of cooling and heating between 433 and 273 K at a rate of ± 5 K/min (Figure S8). The molecular characteristics of all polymers used in this study are summarized in Table 1.

Measurement of the Fluorescence Intensities from FCVJ-Loaded Homopolymers in the Neat State and FCVJ-Loaded PS-PEG Diblock Copolymer Micelles in Water. The following homopolymers were studied: PS_{20} ($M_n=2.1~kDa$, RAFT synthesized), PS_{59} ($M_n=6.1~kDa$, RAFT synthesized), PiBMA₂₄ ($M_n=3.4~kDa$, RAFT synthesized), and $PVAc_{506}$ ($M_n=43.5~kDa$, purchased from Alfa Aesar). FCVJ-loaded samples were prepared as follows. 2 g of polymer was added to 2 mL of a premade 0.1 mg/mL FCVJ solution in chloroform. The mixture was homogenized by vortexing for 1 min. Then, the solvent was removed via vacuum drying at 120 °C and 20 mmHg for 4 h to produce FCVJ-loaded polymer pellets having an FCVJ loading ratio of 0.01 wt %. For fluorescence measurements, FCVJ-loaded polymer pellets were packed into a glass cuvette and melted at 150 °C under vacuum for 8 h to form a compact mass within the cuvette.

Fluorescence intensities from FCVJ-loaded homopolymer samples were measured using an Agilent Technology Cary Eclipse fluorescence spectrophotometer equipped with a Peltier temperature control system. Fluorescence spectra were initially scanned at various excitation and emission wavelengths in order to identify optimal excitation/emission wavelengths that give the maximum fluorescence intensity for each sample (Table 2). Fluorescence intensities were measured at these wavelength settings at designated temperatures during a heating/cooling cycle between 283 and 363 K. At each measurement temperature, the sample was equilibrated for 5 min prior to the measurement of fluorescence intensity. The overall

apparent heating/cooling rate was 0.5 K/min. Cooling curves were analyzed for determination of the $T_{\rm g}$.

FCVJ-loaded PS₅₄–PEG₁₁₄ micelles were prepared using the solvent exchange method. A designated amount of FCVJ was added to a 5 wt % PS–PEG solution in acetone to achieve an FCVJ/PS weight ratio of 0.001:0.999. Milli-Q water was added dropwise to this mixture at a rate of 0.3 mL/min until the concentration of PS–PEG reached a value of 0.5 wt %. The solution was dialyzed against water using a regenerated cellulose membrane with a molecular weight cut-off of 50 kDa (Spectrum Labs) to replace acetone with water. 2 mL of the resulting 0.5 wt % FCVJ-loaded PS–PEG micelle solution was used for the measurement of the temperature-dependent fluorescence intensity using the same procedure as described above.

Prediction of FCVJ Fluorescence Intensities Based on the Free Volume Theory of Glass Transition. The fluorescence intensity—temperature (I-T) profiles from FCVJ-loaded polymers were analyzed using the Loutfy model $(eq\ 1)$. This model relates the rate constant for non-radiative decay of a photo-excited rotor (k_{nr}) to the fractional occupied volume (f_0) and fractional free volume (f) of the matrix assuming that the internal rotation is the rate-determining step of the non-radiative decay

$$k_{\rm nr} = k_{\rm rot}^0 \exp(-xf_0/f) \tag{6}$$

where $k_{\rm rot}^{0}$ is the intrinsic rate of the internal rotation of the rotor, and x is a chemistry-dependent constant of the order of unity (called the "coupling parameter"). The fluorescence quantum yield (Φ) , defined as $\Phi \equiv k_{\rm r}/(k_{\rm r}+k_{\rm nr})$, where $k_{\rm r}$ is the radiative decay rate constant, can be approximated as $\Phi \cong k_{\rm r}/k_{\rm nr}$ in the limit $k_{\rm nr} \gg k_{\rm r}$. This approximation is especially true for FCVJ and other julolidine-based molecular rotors. ^{23,64} Using this approximation, eq 6 is rewritten to eq 1 as $\Phi \cong k_{\rm r}/k_{\rm nr}^{0}$ exp (xf_0/f) . Since the fluorescence intensity (I) is proportional to Φ , one obtains

$$\log I \cong C + \log(k_{\rm r}/k_{\rm nr}^0) + x(f_0/f) \tag{7a}$$

where C is a system-specific constant that depends on the absorptivities of the rotor (for instance, FCVJ) and the polymer $(\varepsilon_{\text{abs,FCVJ}} \text{ and } \varepsilon_{\text{abs,pol}}, \text{ respectively})$ and the normal reflectance of the sample $(R = |(n_{\text{pol}} - n_{\text{glass}})/(n_{\text{pol}} + n_{\text{glass}})|^2$ (Fresnel equation) where n_{pol} and n_{glass} denote, respectively, the indices of refraction of the polymer and the glass cuvette). Since the temperature dependence of f^{-1} is much stronger than those of other properties $(\varepsilon_{\text{abs,FCVJ}}, \varepsilon_{\text{abs,pol}}, R, k_r, \text{ and } k_{\text{rot}}^0$ (because of the absence of an energy barrier for the internal rotation in the gaseous state 24,29)), eq 7a can be simplified to

$$\log I \cong C' + x(f_0/f) \tag{7b}$$

where C' is a temperature-independent constant. Since $f_0 \gg f$ at temperatures near T_g eq 7a further reduces to eq 2 upon using the approximation $f_0/f \cong 1/f$.

The intensity—temperature (I-T) profiles from FCVJ-loaded bulk polymers were analyzed using eq 2 (Loutfy model) on the basis of the LCL model-based total free volume definition $(V_{\rm f,tot})$ (Loutfy—LCL fit) and also of the WLF model-type excess free volume definition $(V_{\rm f,exc})$ (Loutfy—WLF fit) (for the estimation of f(T)). The Loutfy—LCL fit analysis (eqs 3a and 3b) was performed over the entire temperature range covering both the glassy and liquid states. The Loutfy—WLF fit analysis (eqs 4a and 4b) was performed only on the liquid-state data (at $T>T_{\rm g}$); specifically, a trial value of $T_{\rm g}$ was initially used to identify an appropriate range of temperature for the fitting analysis (i.e., $T>T_{\rm g}$), and then a revised estimate for $T_{\rm g}$ was obtained as the temperature at which the model deviates from experimental data; this process was iterated until the value of $T_{\rm g}$ converged to within a reasonable limit.

The I-T profile from FCVJ-loaded PS₅₄–PEG₁₁₄ micelles was analyzed by additionally incorporating a finite distribution of $T_{\rm g}$ values into the Loutfy–LCL model. For simplicity, we assumed that the $T_{\rm g}$ distribution is a step function; that is, $P(T_{\rm g}) = (T_{\rm g,max} - T_{\rm g,min})^{-1}$ (= const.) for $T_{\rm g,max} < T_{\rm g} < T_{\rm g,min}$, and $P(T_{\rm g}) = 0$ for $T_{\rm g} < T_{\rm g,min}$ or $T_{\rm g} > T_{\rm g,max}$. Each volume element within the core domain has a different value of $T_{\rm g}$ and accordingly a different value of $f_{\rm g}$ (the fractional free

volume at $T_{\rm g}$). To calculate the value of $f_{\rm g}$ at a given $T_{\rm g}$, we used the empirical relation suggested by White and Lipson: $^{20}f_{\rm g}(T_{\rm g})=aT_{\rm g}+b$ where $a=3.31\times 10^{-4}~{\rm K}^{-1}$ and $b=-1.49\times 10^{-2}$. At $T_{\rm r}$ volume elements having $T_{\rm g}>T$ would be in the glass state (characterized by $\alpha_{\rm G}$), whereas volume elements having $T_{\rm g}<T$ would be in the liquid state (characterized by $\alpha_{\rm L}$). The total free volume of the glassy volume elements is given as

$$V_{f,G}(T) = V \int_{T}^{T_{g,max}} P(T_g) [f_g(T_g) + \alpha_G(T - T_g)] dT_g \text{ (for } T$$

$$< T_{g,max})$$

Therefore, the total fractional free volume of the glassy elements is

$$f_{\rm G}(T) \equiv \frac{V_{\rm f,G}(T)}{V} = \int_{T}^{T_{\rm g,max}} P(T_{\rm g}) [(a - \alpha_{\rm G})T_{\rm g} + \alpha_{\rm G}T + b] dT_{\rm g}$$
(for $T < T_{\rm g,max}$)
(8a

Similarly, the total fractional free volume of the liquid elements is

$$\begin{split} f_{\rm L}(T) &\equiv \frac{V_{\rm f,L}(T)}{V} = \int_{T_{\rm g,min}}^T P(T_{\rm g})[(a-\alpha_{\rm L})T_{\rm g} + \alpha_{\rm L}T + b] \mathrm{d}T_{\rm g} \\ & (\text{for } T > T_{\rm g,min}) \end{split} \tag{8b}$$

The total fractional free volume of the entire system, $f(T) = f_G(T) + f_L(T)$, is the quantity that determines the fluorescence intensity. Substitution of $P(T_g) = (T_{g,max} - T_{g,min})^{-1}$ into eqs 8a and 8b gives

$$\begin{split} f(T) &= (aT_{\rm g,m} + b) + \frac{\alpha_{\rm L} - \alpha_{\rm G}}{2\Delta T_{\rm g}} (T - T_{\rm g,m})^2 \\ &+ \frac{\alpha_{\rm L} + \alpha_{\rm G}}{2} (T - T_{\rm g,m}) + \frac{\alpha_{\rm L} - \alpha_{\rm G}}{8} \Delta T_{\rm g} \text{ (for } T_{\rm g,min} < T \\ &< T_{\rm g,max}) \end{split}$$

where $T_{\rm g,m}=(T_{\rm g,min}+T_{\rm g,max})/2$, and $\Delta T_{\rm g}=(T_{\rm g,max}-T_{\rm g,min})$. It follows from eq 9 that $f(T_{\rm g,min})=f_{\rm g}(T_{\rm g,m})+\alpha_{\rm G}(T_{\rm g,min}-T_{\rm g,m})$, and $f(T_{\rm g,max})=f_{\rm g}(T_{\rm g,m})+\alpha_{\rm L}(T_{\rm g,max}-T_{\rm g,m})$. Also, it is trivial to show that eq 9 reduces to eqs 3a and 3b when there only exists a single $T_{\rm g}$ (= $T_{\rm g,m}$). The fluorescence data from FCVJ-loaded PS₅₄–PEG₁₁₄ micelles in water (Figure 6b) were fitted with eqs 2 and 9 using $T_{\rm g,min}$, $T_{\rm g,max}$, x, and C' as adjustable parameters.

All-Atom MD Simulation. Atomistic MD simulation of PS_{20} was conducted using GROMACS. The initial density of the amorphous PS mixture was arbitrarily set at 1.0 g/cm³. The interactions between PS chains were modeled using OPLS-AA parameters. The long-range Coulombic interactions were treated using the particle mesh Ewald summation method. 69,70 The simulation box was composed of 20 PS₂₀ chains. From a random initial configuration of the system, the energy was minimized to obtain a stable polymer melt structure. The system was then stabilized at a temperature of 460 K and a pressure of 1 bar by NPT simulation using a velocity-rescale thermostat and the Berendsen pressure coupling method for 10 ns. 71,72 Afterwards, the system was further equilibrated by NPT simulation using the Nose-Hoover temperature coupling method and the Parrinello-Rahman barostat for 10 ns to obtain the most stable liquid polymer structure. 73,74 After this equilibration, the density of the system was 0.94 g/cm³. Using the same thermostat and barostat settings, a stepwise cooling procedure was conducted to study the behavior of PS₂₀. First, the temperature was linearly decreased by 20 K in 5 ns. Next, an additional equilibration was performed for 5 ns at that temperature to measure the thermodynamic properties.

ASSOCIATED CONTENT

Supporting Information

The Supporting Information is available free of charge at https://pubs.acs.org/doi/10.1021/acs.macromol.3c00968.

Representative fluorescence emission spectra of FCVJ-loaded matrices (Figure S1); Arrhenius-type representation of the fluorescence intensities (Figure S2); derivative analysis of the fluorescence intensity for FCVJ-loaded micelles (Figure S3); synthetic scheme, NMR, and fluorescence spectrum of FCVJ (Figure S4); molecular structures and NMR spectra of PS and PiBMA (Figures S5 and S6); GPC and DSC traces of the polymers (Figures S7 and S8) (PDF)

AUTHOR INFORMATION

Corresponding Authors

YongJoo Kim — Department of Materials Science and Engineering, Kookmin University, Seoul 02707, Republic of Korea; orcid.org/0000-0002-6037-7243; Phone: +82-2-910-4685; Email: cjyjee@kookmin.ac.kr

Won Bo Lee — School of Chemical and Biological Engineering, Seoul National University, Seoul 08826, Republic of Korea; orcid.org/0000-0001-7801-083X; Phone: +82-2-880-7076; Email: wblee@snu.ac.kr

You-Yeon Won — Davidson School of Chemical Engineering, Purdue University, West Lafayette, Indiana 47907, United States; Purdue University Center for Cancer Research, Purdue University, West Lafayette, Indiana 47906, United States; orcid.org/0000-0002-8347-6375; Phone: +1-765-494-4077; Email: yywon@purdue.edu; Fax: +1-765-494-0805

Authors

Seyoung Kim — Davidson School of Chemical Engineering, Purdue University, West Lafayette, Indiana 47907, United States; Department of Polymer Science and Engineering, Dankook University, Yongin, Gyeonggi 16890, Republic of Korea

Minhwan Lee − School of Chemical and Biological Engineering, Seoul National University, Seoul 08826, Republic of Korea; oocid.org/0000-0001-9875-713X

Hyun Chang Kim – Davidson School of Chemical Engineering, Purdue University, West Lafayette, Indiana 47907, United States

Complete contact information is available at: https://pubs.acs.org/10.1021/acs.macromol.3c00968

Notes

The authors declare no competing financial interest.

ACKNOWLEDGMENTS

The authors are grateful for funding from ACS PRF (60233-ND7) and NSF (CBET-2211843). The authors also acknowledge support from the Purdue University Center for Cancer Research (PCCR) via an NIH NCI grant (P30 CA023168), which supports the campus-wide NMR shared resources that were utilized in this study. We would also like to thank Prof. Chongli Yuan in the Davidson School of Chemical Engineering at Purdue University for allowing us to use their fluorescence spectrophotometer instrument. This study was presented as a poster at 2023 APS March Meeting. We are grateful to Dr. Ron White from Dartmouth College (the authors of refs 20 61, and 62), who visited our poster and gave many insightful comments.

REFERENCES

- (1) Haidekker, M. A.; Theodorakis, E. A. Environment-Sensitive Behavior of Fluorescent Molecular Rotors. *J. Biol. Eng.* **2010**, *4*, 11–14.
- (2) Burroughs, M. J.; Christie, D.; Gray, L. A. G.; Chowdhury, M.; Priestley, R. D. 21st Century Advances in Fluorescence Techniques to Characterize Glass-Forming Polymers at the Nanoscale. *Macromol. Chem. Phys.* **2018**, 219, 1700368.
- (3) Loutfy, R. O.; Arnold, B. A. Effect of Viscosity and Temperature on Torsional Relaxation of Molecular Rotors. *J. Phys. Chem.* **1982**, *86*, 4205–4211.
- (4) Paul, A.; Samanta, A. Free Volume Dependence of the Internal Rotation of a Molecular Rotor Probe in Room Temperature Ionic Liquids. *J. Phys. Chem. B* **2008**, *112*, 16626–16632.
- (5) Howell, S.; Dakanali, M.; Theodorakis, E. A.; Haidekker, M. A. Intrinsic and Extrinsic Temperature-Dependency of Viscosity-Sensitive Fluorescent Molecular Rotors. *J. Fluoresc.* **2012**, *22*, 457–465
- (6) Meyer, E. F.; Jamieson, A. M.; Simha, R.; Palmen, J. H. M.; Booij, H. C.; Maurer, F. H. J. Free Volume Changes in Polyvinyl Acetate Measured by Fluorescence Spectroscopy. *Polymer* **1990**, *31*, 243–247.
- (7) Royal, J. S.; Torkelson, J. M. Physical Aging Effects on Molecular-Scale Polymer Relaxations Monitored with Mobility-Sensitive Fluorescent Molecules. *Macromolecules* **1993**, *26*, 5331–5335.
- (8) Priestley, R. D.; Ellison, C. J.; Broadbelt, L. J.; Torkelson, J. M. Structural Relaxation of Polymer Glasses at Surfaces, Interfaces, and In Between. *Science* **2005**, *309*, 456–459.
- (9) Mirzahossein, E.; Grzelka, M.; Pan, Z.; Demirkurt, B.; Habibi, M.; Brouwer, A. M.; Bonn, D. Molecular Rotors to Probe the Local Viscosity of a Polymer Glass. *J. Chem. Phys.* **2022**, *156*, 174901.
- (10) Ellison, C. J.; Torkelson, J. M. Sensing the Glass Transition in Thin and Ultrathin Polymer Films via Fluorescence Probes and Labels. J. Polym. Sci., Part B: Polym. Phys. 2002, 40, 2745–2758.
- (11) Ellison, C. J.; Kim, S. D.; Hall, D. B.; Torkelson, J. Confinement and processing effects on glass transition temperature and physical aging in ultrathin polymer films: Novel fluorescence measurements. *Eur. Phys. J. E* **2002**, *8*, 155–166.
- (12) Rittigstein, P.; Priestley, R. D.; Broadbelt, L. J.; Torkelson, J. M. Model Polymer Nanocomposites Provide an Understanding of Confinement Effects in Real Nanocomposites. *Nat. Mater.* **2007**, *6*, 278–282.
- (13) Jones, P. F.; Siegel, S. Intersystem Crossing in Pyrene-H10 and Pyrene-D10. Chem. Phys. Lett. 1968, 2, 486–488.
- (14) Yao, C.; Kraatz, H. B.; Steer, R. P. Photophysics of Pyrene-Labelled Compounds of Biophysical Interest. *Photochem. Photobiol. Sci.* **2005**, *4*, 191–199.
- (15) Hooker, J. C.; Torkelson, J. M. Coupling of Probe Reorientation Dynamics and Rotor Motions to Polymer Relaxation As Sensed by Second Harmonic Generation and Fluorescence. *Macromolecules* **1995**, *28*, 7683–7692.
- (16) Loutfy, R. O. High-conversion polymerization of fluorescence probes. 1. Polymerization of methyl methacrylate. *Macromolecules* **1981**, *14*, 270–275.
- (17) Doolittle, A. K. Studies in Newtonian Flow. II. The Dependence of the Viscosity of Liquids on Free-Space. *J. Appl. Phys.* **1951**, 22, 1471–1475.
- (18) Mundra, M. K.; Ellison, C. J.; Rittigstein, P.; Torkelson, J. M. Fluorescence Studies of Confinement in Polymer Films and Nanocomposites: Glass Transition Temperature, Plasticizer Effects, and Sensitivity to Stress Relaxation and Local Polarity. *Eur. Phys. J.: Spec. Top.* **2007**, *141*, 143–151.
- (19) Priestley, R. D.; Mundra, M. K.; Barnett, N. J.; Broadbelt, L. J.; Torkelson, J. M. Effects of Nanoscale Confinement and Interfaces on the Glass Transition Temperatures of a Series of Poly(n-Methacrylate) Films. *Aust. J. Chem.* **2007**, *60*, 765–771.

- (20) White, R. P.; Lipson, J. E. G. Polymer Free Volume and Its Connection to the Glass Transition. *Macromolecules* **2016**, *49*, 3987–4007.
- (21) Haidekker, M. A.; Ling, T.; Anglo, M.; Stevens, H. Y.; Frangos, J. A.; Theodorakis, E. A. New Fluorescent Probes for the Measurement of Cell Membrane Viscosity. *Chem. Biol.* **2001**, *8*, 123–131.
- (22) Zhu, D.; Haidekker, M. A.; Lee, J. S.; Won, Y. Y.; Lee, J. C. M. Application of Molecular Rotors to the Determination of the Molecular Weight Dependence of Viscosity in Polymer Melts. *Macromolecules* **2007**, *40*, 7730–7732.
- (23) Jee, A. Y.; Bae, E.; Lee, M. Internal Twisting Dynamics of Dicyanovinyljulolidine in Polymers. *J. Phys. Chem. B* **2009**, *113*, 16508–16512.
- (24) Swalina, C.; Maroncelli, M. Nonradiative Deactivation in Benzylidene Malononitriles. *J. Phys. Chem. C* **2010**, *114*, 5602–5610. (25) Lord, S. J.; Conley, N. R.; Lee, H. L. D.; Nishimura, S. Y.; Pomerantz, A. K.; Willets, K. A.; Lu, Z.; Wang, H.; Liu, N.; Samuel, R.; Weber, R.; Semyonov, A.; He, M.; Twieg, R. J.; Moerner, W. E.
- DCDHF Fluorophores for Single-Molecule Imaging in Cells. *ChemPhysChem* **2009**, *10*, 55–65.

 (26) Mudliar, N. H.; Sadhu, B.; Pettiwala, A. M.; Singh, P. K. Evaluation of an Ultrafast Molecular Rotor, Auramine O, as a
- 10507. (27) Hong, Y.; Lam, J. W. Y.; Tang, B. Z. Aggregation-Induced Emission. *Chem. Soc. Rev.* **2011**, *40*, 5361–5388.

Fluorescent Amyloid Marker. J. Phys. Chem. B 2016, 120, 10496-

- (28) Zhang, W.; Lan, Z.; Sun, Z.; Gaffney, K. J. Resolving Photo-Induced Twisted Intramolecular Charge Transfer with Vibrational Anisotropy and TDDFT. *J. Phys. Chem. B* **2012**, *116*, 11527–11536.
- (29) Allen, B. D.; Benniston, A. C.; Harriman, A.; Rostron, S. A.; Yu, C. The Photophysical Properties of a Julolidene-Based Molecular Rotor. *Phys. Chem. Chem. Phys.* **2005**, *7*, 3035–3040.
- (30) Katsumata, R.; Dulaney, A. R.; Kim, C.; Ellison, C. J. Glass Transition and Self-Diffusion of Unentangled Polymer Melts Nanoconfined by Different Interfaces. *Macromolecules* **2018**, *51*, 7509–7517.
- (31) Ehlich, D.; Sillescu, H. Tracer Diffusion at the Glass Transition. *Macromolecules* **1990**, 23, 1600–1610.
- (32) Rogers, S. S.; Mandelkern, L. Glass Transitions of the Poly-(n-Alkyl Methacrylates). *J. Phys. Chem.* **1957**, *61*, 985–991.
- (33) Wood, L. A. Glass Transition Temperatures of Copolymers. J. Polym. Sci. 1958, 31, 459–468.
- (34) Sasabe, H.; Moynihan, C. T. Structural Relaxation in Poly(Vinyl Acetate). *J. Polym. Sci., Polym. Phys. Ed.* **1978**, *16*, 1447–1457.
- (35) Skrabania, K.; Miasnikova, A.; Bivigou-Koumba, A. M.; Zehm, D.; Laschewsky, A. Examining the UV-Vis Absorption of RAFT Chain Transfer Agents and Their Use for Polymer Analysis. *Polym. Chem.* **2011**, *2*, 2074–2083.
- (36) Lodge, T. P.; Hiemenz, P. C. Polymer Chemistry, 3rd ed.; CRC Press: Boca Raton, 2020.
- (37) Larini, L.; Ottochian, A.; De Michele, C.; Leporini, D. Universal Scaling between Structural Relaxation and Vibrational Dynamics in Glass-Forming Liquids and Polymers. *Nat. Phys.* **2008**, *4*, 42–45.
- (38) Barrat, J.-L.; Baschnagel, J.; Lyulin, A. Molecular Dynamics Simulations of Glassy Polymers. *Soft Matter* **2010**, *6*, 3430–3446.
- (39) Jin, H.; Liang, M.; Arzhantsev, S.; Li, X.; Maroncelli, M. Photophysical Characterization of Benzylidene Malononitriles as Probes of Solvent Friction. *J. Phys. Chem. B* **2010**, *114*, 7565–7578.
- (40) Yang, S.; Han, K. Effects of Solvent Dielectric Constant and Viscosity on Two Rotational Relaxation Paths of Excited 9-(Dicyanovinyl) Julolidine. *J. Phys. Chem. A* **2016**, *120*, 4961–4965.
- (41) Chen, X.; Ye, Y.; Hao, L. Atomistic Picture of Isothermal Volume Relaxation Behavior of Atactic Polystyrene Glass Provided by a Molecular Dynamics Simulation. *J. Chem. Phys.* **2012**, *137*, 044907.
- (42) Xie, S.-J.; Qian, H.-J.; Lu, Z.-Y. The Influence of Internal Rotational Barriers and Temperature on Static and Dynamic

- Properties of Bulk Atactic Polystyrene. J. Chem. Phys. 2012, 137, 244903.
- (43) Roland, C. M.; Ngai, K. L.; Santangelo, P. G.; Qiu, X.; Ediger, M. D.; Plazek, D. J. Temperature Dependence of Segmental and Terminal Relaxation in Atactic Polypropylene Melts. *Macromolecules* **2001**, *34*, 6159–6160.
- (44) Qiu, Z.; Chu, E. K. K.; Jiang, M.; Gui, C.; Xie, N.; Qin, W.; Alam, P.; Kwok, R. T. K.; Lam, J. W. Y.; Tang, B. Z. A Simple and Sensitive Method for an Important Physical Parameter: Reliable Measurement of Glass Transition Temperature by AIEgens. *Macromolecules* **2017**, *50*, 7620–7627.
- (45) Kumaraswamy, G. N.; Ranganathaiah, C. Free Volume Microprobe Studies on Poly(Methyl Methacrylate)/Poly(Vinyl Chloride) and Poly(Vinyl Chloride)/Polystyrene Blends. *Polym. Eng. Sci.* **2006**, *46*, 1231–1241.
- (46) Kobayashi, Y.; Zheng, W.; Meyer, E. F.; McGervey, J. D.; Jamieson, A. M.; Simha, R. Free volume and physical aging of poly(vinyl acetate) studied by positron annihilation. *Macromolecules* **1989**, *22*, 2302–2306.
- (47) Kilburn, D.; Dlubek, G.; Pionteck, J.; Alam, M. A. Free Volume in Poly(n-Alkyl Methacrylate)s from Positron Lifetime and PVT Experiments and Its Relation to the Structural Relaxation. *Polymer* **2006**, *47*, 7774–7785.
- (48) Koenig, M.; Bottari, G.; Brancato, G.; Barone, V.; Guldi, D. M.; Torres, T. Unraveling the Peculiar Modus Operandi of a New Class of Solvatochromic Fluorescent Molecular Rotors by Spectroscopic and Quantum Mechanical Methods. *Chem. Sci.* **2013**, *4*, 2502–2511.
- (49) Kim, H. C.; Suresh, M. V.; Singh, V. V.; Arick, D. Q.; Machado-Aranda, D. A.; Raghavendran, K.; Won, Y.-Y. Polymer Lung Surfactants. *ACS Appl. Bio Mater.* **2018**, *1*, 581–592.
- (50) Kim, S.; Fesenmeier, D. J.; Park, S.; Torregrosa-Allen, S. E.; Elzey, B. D.; Won, Y. Y. Pulmonary Pharmacokinetics of Polymer Lung Surfactants Following Pharyngeal Administration in Mice. *Biomacromolecules* **2022**, 23, 2471–2484.
- (51) Fesenmeier, D. J.; Suresh, M. V.; Kim, S.; Park, S.; Raghavendran, K.; Won, Y.-Y. Polymer Lung Surfactants Attenuate Direct Lung Injury in Mice. ACS Biomater. Sci. Eng. 2023, 9, 2716–2730.
- (52) Park, K.; Otte, A.; Sharifi, F.; Garner, J.; Skidmore, S.; Park, H.; Jhon, Y. K.; Qin, B.; Wang, Y. Potential Roles of the Glass Transition Temperature of PLGA Microparticles in Drug Release Kinetics. *Mol. Pharm.* 2021, 18, 18–32.
- (53) Roth, C. B. Polymers under Nanoconfinement: Where Are We Now in Understanding Local Property Changes? *Chem. Soc. Rev.* **2021**, *50*, 8050–8066.
- (54) Zhang, C.; Guo, Y.; Priestley, R. D. Confined Glassy Properties of Polymer Nanoparticles. *J. Polym. Sci., Part B: Polym. Phys.* **2013**, *51*, 574–586.
- (55) Feng, S.; Li, Z.; Liu, R.; Mai, B.; Wu, Q.; Liang, G.; Gao, H.; Zhu, F. Glass Transition of Polystyrene Nanospheres under Different Confined Environments in Aqueous Dispersions. *Soft Matter* **2013**, *9*, 4614.
- (56) Wei, W.-C.; Feng, S.; Zheng, C. X.; Liang, G. D.; Gao, H. Y.; Wu, Q.; Zhu, F. M. Glass Transition and Quantum Yield for Fluorescent Labelled Polystyrene Core-Forming Block in Self-Assembled Nanomicelles of Amphiphilic Diblock Copolymers. *J. Polym. Res.* **2015**, *22*, 212–218.
- (57) Christie, D.; Zhang, C.; Fu, J.; Koel, B.; Priestley, R. D. Glass Transition Temperature of Colloidal Polystyrene Dispersed in Various Liquids. *J. Polym. Sci., Part B: Polym. Phys.* **2016**, *54*, 1776–1783.
- (58) Ellison, C. J.; Torkelson, J. M. The Distribution of Glass-Transition Temperatures in Nanoscopically Confined Glass Formers. *Nat. Mater.* **2003**, *2*, 695–700.
- (59) Baglay, R. R.; Roth, C. B. Local Glass Transition Temperature Tg(z) of Polystyrene next to Different Polymers: Hard vs. Soft Confinement. *J. Chem. Phys.* **2017**, *146*, 203307.
- (60) Priestley, R. D.; Broadbelt, L. J.; Torkelson, J. M. Physical Aging of Ultrathin Polymer Films above and below the Bulk Glass

Transition Temperature: Effects of Attractive vs Neutral Polymer—Substrate Interactions Measured by Fluorescence. *Macromolecules* **2005**, *38*, 654–657.

- (61) White, R. P.; Lipson, J. E. G. A Simple New Way to Account for Free Volume in Glassy Dynamics: Model-Free Estimation of the Close-Packed Volume from PVT Data. *J. Phys. Chem. B* **2021**, *125*, 4221–4231.
- (62) White, R. P.; Lipson, J. E. G. The Cooperative Free Volume Rate Model for Segmental Dynamics: Application to Glass-Forming Liquids and Connections with the Density Scaling Approach. *Eur. Phys. J. E* **2019**, 42, 100.
- (63) Neises, B.; Steglich, W. Simple Method for the Esterification of Carboxylic Acids. *Angew. Chem., Int. Ed.* **1978**, *17*, 522–524.
- (64) Loutfy, R. O. Effect of Polystyrene Molecular Weight on the Fluorescence of Molecular Rotors. *Macromolecules* **1983**, *16*, 678–680
- (65) Berendsen, H. J. C.; van der Spoel, D.; van Drunen, R. GROMACS: A Message-Passing Parallel Molecular Dynamics Implementation. *Comput. Phys. Commun.* **1995**, *91*, 43–56.
- (66) Lindahl, E.; Hess, B.; van der Spoel, D. GROMACS 3.0: A Package for Molecular Simulation and Trajectory Analysis. *Mol. Model. Annu.* **2001**, *7*, 306–317.
- (67) Van Der Spoel, D.; Lindahl, E.; Hess, B.; Groenhof, G.; Mark, A. E.; Berendsen, H. J. C. GROMACS: Fast, Flexible, and Free. *J. Comput. Chem.* **2005**, 26, 1701–1718.
- (68) Hess, B.; Kutzner, C.; Van Der Spoel, D.; Lindahl, E. GROMACS 4: Algorithms for Highly Efficient, Load-Balanced, and Scalable Molecular Simulation. *J. Chem. Theory Comput.* **2008**, *4*, 435–447.
- (69) Jorgensen, W. L.; Maxwell, D. S.; Tirado-Rives, J. Development and Testing of the OPLS All-Atom Force Field on Conformational Energetics and Properties of Organic Liquids. *J. Am. Chem. Soc.* **1996**, 118, 11225–11236.
- (70) Darden, T.; York, D.; Pedersen, L. Particle Mesh Ewald: An N-log(N) Method for Ewald Sums in Large Systems. *J. Chem. Phys.* **1993**, *98*, 10089–10092.
- (71) Bussi, G.; Donadio, D.; Parrinello, M. Canonical Sampling through Velocity Rescaling. *J. Chem. Phys.* **2007**, *126*, 014101.
- (72) Berendsen, H. J. C.; Postma, J. P. M.; van Gunsteren, W. F.; DiNola, A.; Haak, J. R. Molecular Dynamics with Coupling to an External Bath. *J. Chem. Phys.* **1984**, *81*, 3684–3690.
- (73) Hoover, W. G. Canonical Dynamics: Equilibrium Phase-Space Distributions. *Phys. Rev. A* **1985**, *31*, 1695–1697.
- (74) Nosé, S. A. A molecular dynamics method for simulations in the canonical ensemble. *Mol. Phys.* **1984**, *52*, 255–268.